Reversible Burst of Transcriptional Changes during Induction of Crassulacean Acid Metabolism in *Talinum triangulare*[1][OPEN]

Dominik Brilhaus, Andrea Bräutigam, Tabea Mettler-Altmann, Klaus Winter, and Andreas P.M. Weber*

Institute of Plant Biochemistry, Cluster of Excellence on Plant Sciences (CEPLAS), Heinrich-Heine-University, D–40225 Düsseldorf, Germany (D.B., A.B., T.M.-A., A.P.M.W.); and Smithsonian Tropical Research Institute, Balboa, Ancón, Republic of Panama (K.W.)

ORCID IDS: 0000-0001-9021-3197 (D.B.); 0000-0002-5309-0527 (A.B.); 0000-0002-9161-4889 (T.M.-A.); 0000-0003-0970-4672 (A.P.M.W.).

Drought tolerance is a key factor for agriculture in the 21st century as it is a major determinant of plant survival in natural ecosystems as well as crop productivity. Plants have evolved a range of mechanisms to cope with drought, including a specialized type of photosynthesis termed Crassulacean acid metabolism (CAM). CAM is associated with stomatal closure during the day as atmospheric CO_2 is assimilated primarily during the night, thus reducing transpirational water loss. The tropical herbaceous perennial species *Talinum triangulare* is capable of transitioning, in a facultative, reversible manner, from C_3 photosynthesis to weakly expressed CAM in response to drought stress. The transcriptional regulation of this transition has been studied. Combining mRNA-Seq with targeted metabolite measurements, we found highly elevated levels of CAM-cycle enzyme transcripts and their metabolic products in *T. triangulare* leaves upon water deprivation. The carbohydrate metabolism is rewired to reduce the use of reserves for growth to support the CAM-cycle and the synthesis of compatible solutes. This large-scale expression dataset of drought-induced CAM demonstrates transcriptional regulation of the C_3–CAM transition. We identified candidate transcription factors to mediate this photosynthetic plasticity, which may contribute in the future to the design of more drought-tolerant crops via engineered CAM.

Drought is a major determinant of both plant survival in natural ecosystems and plant productivity in agriculture (Lobell and Gourdji, 2012). Plants have evolved a range of physiological and nonphysiological traits to cope with water deficit stress (Bartels and Sunkar, 2005). Drought adaptation includes leaf shedding in perennials or completing the life cycle while enough water is present in annuals. Few species (e.g. so-called resurrection plants) tolerate extreme dehydration (Ingram and Bartels, 1996) and resume life upon water resupply. Other plants have evolved strategies to cope with drought, such as specialized biochemical pathways, cells, tissues, and organs to survive water scarcity by mitigating the reduction in tissue water loss (Chaves et al., 2003).

Water limitation sensed in the roots or leaves triggers stress signals, which include but are not limited to abscisic acid (ABA; Bray, 1997; Zhu, 2002; Chaves et al., 2003; Bartels and Sunkar, 2005). The immediate consequence of an ABA signal is stomatal closure (Kollist et al., 2014). This can lead to short-term carbon dioxide (CO_2) limitation of photosynthesis, potentially causing oxidative stress, which is mitigated by protective systems (Bartels and Sunkar, 2005; Flexas et al., 2006). The accumulation of compatible solutes is induced to protect the cellular machinery from consequences of leaf water loss and to lower the water potential of the leaf (Hare et al., 1998). These molecules include sugars, such as raffinose, trehalose, and Suc; sugar alcohols like mannitol and inositol; and amino acids and their derivatives, such as Pro or Gly betaine (Hare et al., 1998; Elbein et al., 2003). The signaling cascade has been largely elucidated. ABA is bound by the PYRABACTIN RESISTANCE1 AND PYR1-LIKE REGULATORY COMPONENTS OF ABA RECEPTOR family proteins, which upon binding inhibit the TYPE 2C AND TYPE 2A PROTEIN PHOSPHATASES (PP2C; Cutler et al., 2010). This inhibition, in turn, relieves the inhibition of the protein kinase OPEN STOMATA1 and other kinases, which phosphorylate their targets including the ABA RESPONSIVE ELEMENT BINDING FACTORS. They finally trigger ABA-responsive gene expression (Park et al., 2009). The capability to reduce leaf water loss is variable between species, and leaf water loss exceeding a threshold irreversibly damages a leaf (Lawlor and Cornic, 2002).

[1] This work was supported by the International Graduate Program for Plant Science (iGRAD-Plant; to D.B.) and grants from Deutsche Forschungsgemeinschaft (EXC 1028; IRTG 1525 to A.P.M.W.). K.W. was supported by the Smithsonian Tropical Research Institute.

* Address correspondence to andreas.weber@hhu.de.

The author responsible for distribution of materials integral to the findings presented in this article in accordance with the policy described in the Instructions for Authors (www.plantphysiol.org) is: Andreas P.M. Weber (andreas.weber@hhu.de).

D.B., A.B., T.M.-A., K.W., and A.P.M.W. designed the research; D.B., K.W., and T.M.-A. performed the research; D.B., A.B., and T.M.-A. analyzed data; D.B., A.B., T.M.-A., K.W., and A.P.M.W. wrote the article.

[OPEN] This article is available without a subscription.

www.plantphysiol.org/cgi/doi/10.1104/pp.15.01076

The tropical herbaceous dicot *Talinum triangulare* (Jacq). Willd. [according to The Plant List Kew now considered a synonym of the accepted name *Talinum fruticosum* (L.) Juss., but referred to within this work as *T. triangulare* to relate to extensive ecophysiological work on "*T. triangulare*" by Herrera et al. (1991), Taisma and Herrera (1998), Herrera (1999), Taisma and Herrera (2003), and Herrera et al. (2015)], in the family *Talinaceae* (formerly *Portulacaceae*), responds to intermittent drought (Harris and Martin, 1991; Herrera et al., 1991) in two ways. Leaves change from a horizontal to a vertical orientation and exhibit leaf-rolling (Herrera et al., 1991; Taisma and Herrera, 1998; Herrera, 1999). Leaves induce Crassulacean acid metabolism (CAM) in a reversible, facultative manner (Taisma and Herrera, 1998; Herrera, 2009; Winter and Holtum, 2014; Herrera et al., 2015).

CAM is a carbon concentrating mechanism allowing stomatal closure during the day as atmospheric CO_2 is primarily assimilated during the night by PHOSPHO-*ENOL*PYRUVATE CARBOXYLASE (PEPC; Osmond, 1978). The produced organic acids (mainly malic acid) are decarboxylated during the following day to provide CO_2 for the secondary, light-driven carboxylation via Rubisco. The magnitude of CAM varies between and within plant species (Borland et al., 2011). While constitutive CAM plants are ontogenetically determined to engage in this photosynthetic mode at some point in their life cycle, in facultative CAM plants, a transition to CAM occurs in response to water-deficit stress (Winter et al., 2008; Winter and Holtum, 2014). The ability to experimentally control the timing of CAM induction and CAM-to-C_3 reversal makes facultative CAM plants excellent systems to identify key components of CAM.

Extensive physiological, molecular, and mutant-based studies of facultative CAM were focused on, but not restricted to, the halophyte *Mesembryanthemum crystallinum*, and aided to understand central concepts of the CAM-cycle (Winter and von Willert, 1972; Holtum and Winter, 1982; Cushman et al., 2008a). These included a microarray-based large scale gene expression data set (Cushman et al., 2008b), which described major changes in mRNA steady-state levels during the salinity-induced transition from C_3 to CAM. Reversibility of CAM back to C_3 photosynthesis after irrigation was reinitiated has been documented for several species including *T. triangulare* (for review, see Winter and Holtum, 2014). To date, it is not fully understood how this metabolic plasticity is transcriptionally accomplished (Yang et al., 2015). We studied the *T. triangulare* transition from well-watered to water-limited and back to well-watered conditions (1) to test how CAM induction and its reversion are controlled at the level of mRNA abundance and (2) to evaluate CAM- and drought-specific changes in metabolite levels.

RESULTS

Nocturnal Acidification

Following germination, *T. triangulare* was grown well-watered for 28 d. Subsequently, water was withheld for 12 d before rewatering. Fresh weight to dry weight ratio after 4, 9, and 12 d of water deprivation showed slight, continuous (1.1%, 4.8%, and 15.0%, respectively) decreases compared to day 0, which were significant on day 12 (Fig. 1A). Measurements of titratable acidity were used as an indicator of the presence or absence of CAM activity in leaves (Fig. 1B). In well-watered plants, acidity levels were low (10 μmol H^+ g^{-1} fresh weight) and did not change in the course of the night. Withholding water for 4 d did not significantly alter titratable acidity compared to well-watered plants. Significant nocturnal acidification, indicative of CAM, was observed in plants from which water was withheld for 9 and 12 d, consistent with previous findings of Herrera et al. (1991) and Winter and Holtum (2014). Drought stress also resulted in pronounced leaf rolling (Fig. 1C). Following rewatering for 2 d, plants returned to a full C_3 photosynthetic pattern without nocturnal increases in tissue acidity and unrolled leaves (Fig. 1, B and C). However, fresh weight to dry weight ratio was significantly lower (22.7%) compared to day 0 (Fig. 1A).

Changes in Transcript and Metabolite Levels

Samples for mRNA-Seq were taken at midday and midnight prior to the drought treatment (day 0, well-watered), on day 4, day 9, and day 12 of drought, and again 2 d after rewatering (Fig. 2, A and B). Biological triplicates yielded, on average, 40.7 million reads over the time course (Supplemental Table S1). Of those, an average of 52% could be mapped for quantification to the reference genome of Arabidopsis (*Arabidopsis thaliana*; Supplemental Table S1; "Materials and Methods"). The mapped reads matched 16,766 Arabidopsis genes with at least one read per gene. This is comparable to the yield of cross species mapping with equidistant species for both number of genes matched and percentage of mapped reads (Gowik et al., 2011). Within-species mapping on the assembled contigs resulted in 81% mapped reads but indicated that the assembly suffers from the known limitations of transcriptome assembly such as contig fragmentation (Franssen et al., 2011; Supplemental Dataset S2).

Statistical evaluation including multiple hypothesis testing correction (by DESeq2; for details, see "Materials and Methods") identified significantly differential gene expression for 4,628 genes (28% of the whole transcriptome) at midday and 5,191 genes (31% of the transcriptome) at midnight on day 9 as well as 6,143 genes (37% of the transcriptome) at midday and 6,565 genes (39% of the transcriptome) at midnight on day 12 compared to well-watered plants (day 0), i.e. during the 2 d during which pronounced CAM activity was observed (Fig. 2B).

On day 9, 2,117 (12.6%) and 2,213 (13.2%) genes were upregulated, while 2,511 (15%) and 2,978 genes (17.8%) were downregulated at midday and midnight, respectively. On day 12, 2,713 (16.2%) and 2,897 (17.3%) genes were upregulated, while 3,430 (20.5%) and 3,668 genes (21.9%) were downregulated at midday and midnight, respectively. A Venn analysis indicated that 1,634

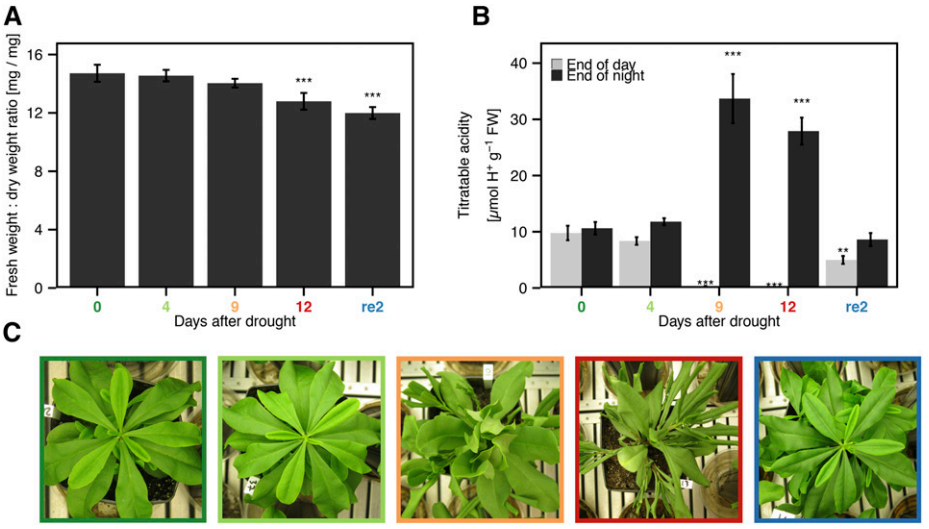

Figure 1. Time course in response to 0 (darkgreen), 4 (light green), 9 (orange), and 12 (red) d of drought and 2 d after rewatering (re2, blue) in *T. triangulare*. A, Fresh weight to dry weight ratio (mean ± SE of leaves harvested at the middle of the day and the middle of the night, $n = 14–16$). B, Levels of titratable acidity of leaves (mean ± SE, $n = 8–16$). C, Representative pictures of plants during the course of the experiment. Asterisks indicate Student's *t* test significance in comparison to day 0 at $***P < 0.001$, $**P < 0.01$, and $*P < 0.05$.

genes and 2,180 genes were shared among the genes up- and downregulated at midday, respectively (Fig. 2B), while at midnight, 1,545 upregulated and 1,865 downregulated genes were shared (Supplemental Fig. S1.). A small percentage (1.9% and 2.1% of upregulated and 1.2% and 1.9% of downregulated genes at midday and midnight, respectively) was exclusively differentially regulated on day 9. On day 4 of water

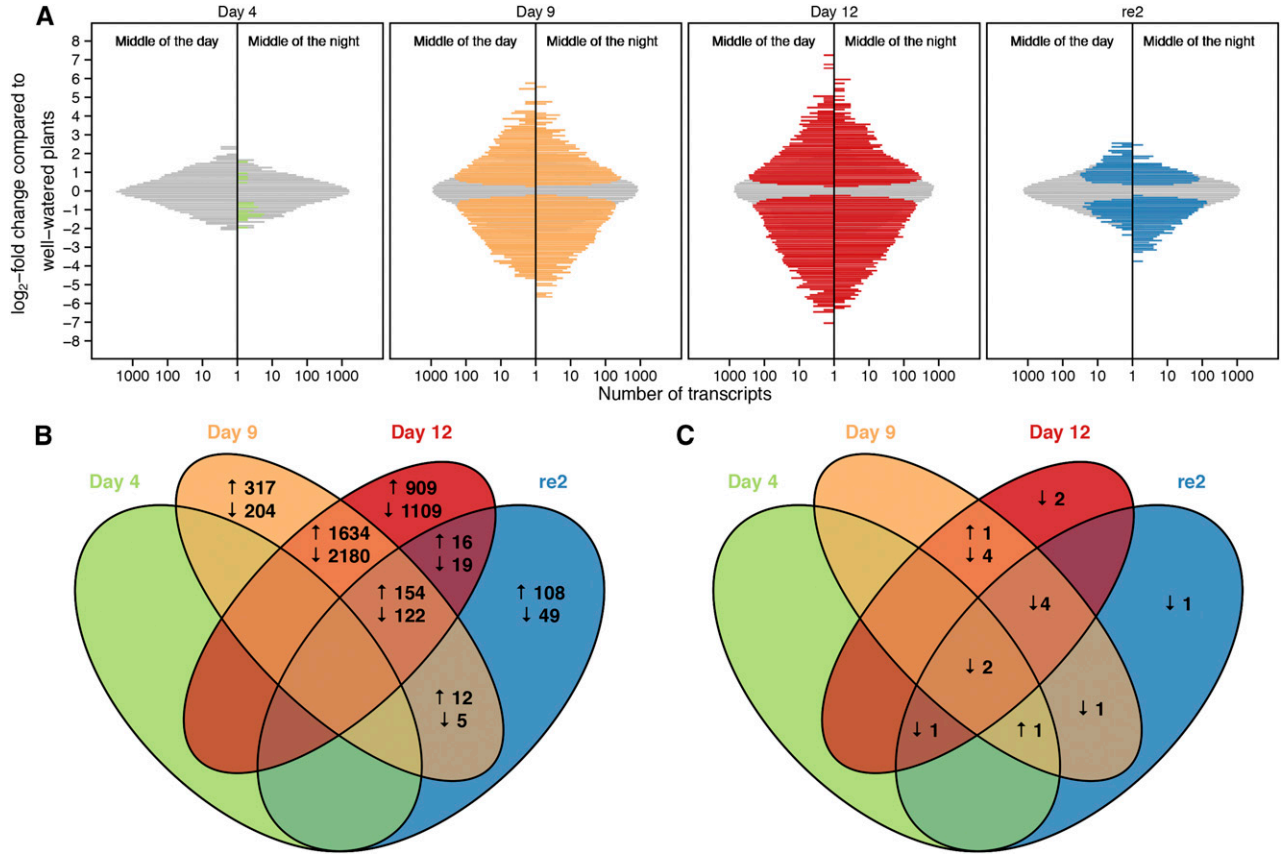

Figure 2. Changes in leaf transcriptomes and metabolomes under varying levels of water availability. A, Histograms of $\log_2$-fold changes in gene expression compared to day 0 ($\log_{10}$-scaled). Colored bars indicate significant changes (DESeq2, $q < 0.01$). B and C, Venn diagrams representing overlapping changes (↑: increased, ↓: depleted) in gene expression (B, DESeq2 $q < 0.01$, $n = 3$, 16,766 genes analyzed in total) or metabolite levels (C, Student's *t* test, $P < 0.05$, $n = 3–4$, 39 metabolites measured in total) at the middle of the day between water-limited stages compared to day 0. See Supplemental Figure S1 for analogous Venn diagrams of changes at the middle of the night.

deprivation, no differentially expressed genes (DEGs) were detectable compared to well-watered conditions at midday, while at midnight 16 genes were up- and 35 were downregulated (Supplemental Fig. S1). Upon rewatering, the number of significantly DEGs was reduced to 485 at midday (3% of the transcriptome) and 1,632 (10% of the transcriptome) at midnight. To compare the changes of steady-state levels of mRNA and metabolites, 39 metabolites were quantified at midday and midnight on days 0, 4, 9, 12, and after rewatering for 2 d (Fig. 2C; Supplemental Fig. S1; Supplemental Table S2). On day 4, nine metabolites were significantly different from well-watered plants at either midday or midnight. In leaves harvested at day 9 and 12, 13 and 14 of the 39 metabolites differed significantly at midday, while 6 and 11 metabolites differed significantly at midnight, respectively. The highest total number of significant changes was observed in rewatered plants, 10 at midday and 16 at midnight compared to day 0. Both the transcriptome analysis and the targeted metabolite profiling showed that transcriptome and metabolome were markedly altered in *T. triangulare* plants, which experience drought. While changes in mRNA abundance were largely reversed upon rewatering (Fig. 2A), the metabolic state remained altered.

CAM-Related Transcriptional Changes

Transcript abundance of known enzymes of the CAM-cycle sensu stricto (i.e. carboxylation and decarboxylation) and sensu lato (i.e. encoding auxiliary steps such as starch turnover and glycolysis for phospho*enol*pyruvate [PEP] generation) were analyzed during C_3-CAM-C_3 transitions. Transcripts encoding four CAM-cycle enzymes sensu stricto, namely PEPC, NADP-MALIC ENZYME (NADP-ME), NAD-MALIC ENZYME (NAD-ME), and PYRUVATE, *ORTHO*PHOSPHATE DIKINASE (PPDK) had higher steady-state levels at both midnight and midday on day 9 and/or day 12 of water-limitation (Fig. 3; Supplemental Dataset S3).

CARBONIC ANHYDRASE (CA) catalyzes the hydration of CO_2 to HCO_3^- at physiological pH and thereby is thought to support providing PEPC with its substrate in CAM plants (Tsuzuki et al., 1982). The gene encoding cytosolic BETA-CARBONIC ANHYDRASE3 (BCA3) was unchanged in expression upon drought but already highly expressed in C_3 conditions (2,498 rpm on day 0). This is in agreement with an earlier study finding no differences in CA activity in *M. crystallinum* in C_3 and CAM mode (Tsuzuki et al., 1982). Two lowly expressed genes encoding CA isoforms (alpha CA3 between 2.7 and 10 rpm and BCA5 between 23.7 and 80.7 rpm) were upregulated at midday on both days. Upregulation of major carbonic anhydrase isoforms as it was found for *M. crystallinum* (Cushman et al., 2008b) could not be detected in *T. triangulare*.

The gene *PPC* encodes PEPC, which catalyzes the CO_2 carboxylation at night. *PPC* was upregulated 25-fold at midnight (to 15,510 rpm, expression rank 4 on day 12) on day 9 and 12, respectively. The coding sequences of *PPC* vary between C_3, C_4, and CAM plants (Bläsing et al., 2000; Paulus et al., 2013). The coding sequences of the four *T. triangulare PPC* contigs with on average at least 100 reads mapped were extracted from the assembly, translated, and aligned with PEPC sequences from various C_3, C_4, and CAM plants (http://www.uniprot.org; Supplemental Fig. S2; Supplemental Table S3). The *T. triangulare* contigs encoding for PEPC showed characteristics of both C_3 and C_4 PEPCs. PEP saturation kinetics are known to be determined by the amino acid at position 780 (counting based on *Zea mays* sequence CAA33317), which in C_4 plants is typically Ser and in C_3 plants Ala (Bläsing et al., 2000). Sensitivity to malate inhibition is determined by the amino acid at position 890, Gly in C_4 plants, and Arg in C_3 plants (Paulus et al., 2013). While at position 890, all contigs encoded for the C_3-typical Arg in *T. triangulare*; at position 780, contig Tt63271 (7,638 rpm at midnight on day 9) and Tt9871_8 (1,198 rpm at midnight on day 12) encoded for the C_3 typical Ala, Tt9871_4 (1,409 rpm at midnight on day 9) and Tt9871_6 (399 rpm at midnight on day 12) encoded for the C_4-typical Ser (Supplemental Fig. S2). Read mapping on the contig level identified all isoforms as upregulated during CAM (Supplemental Table S3); however, it cannot be determined whether Tt63271 and Tt9871_8, Tt9871_4 and Tt9871_6 are alleles or recent duplicates.

Oxaloacetate (OAA) resulting from PEP carboxylation is reduced to malate by MALATE DEHYDROGENASE (MDH). The cytosolic MDH was unchanged but constitutively highly expressed in C_3 conditions (941 rpm at midday on day 0) and during CAM (1,141 rpm, expression rank 110 at midday on day 12). Malate is stored as malic acid in the vacuole during the night (Cheffings et al., 1997). Genes encoding two malate channels of the ALUMINUM-ACTIVATED MALATE TRANSPORTER (ALMT) family were upregulated 6-fold and 28-fold at midnight, but reached only 4 and 19 rpm after upregulation, respectively. While below 1 rpm in abundance at any other day, transcripts encoding the TONOPLAST DICARBOXYLATE TRANSPORTER are detectable on day 12 (MD: 5 rpm, MN: 11 rpm). *VHA-B3*, encoding the subunit B3 of the vacuolar ATPase (V-ATPase), which sustains the electrochemical gradient during import of malic acid (White and Smith, 1989), is the major expressed subunit, being significantly upregulated 2-fold on day 12. Of the 11 other genes encoding for V-ATPase subunits, two were unaltered and eight genes were slightly but significantly downregulated during CAM (Supplemental Table S4). *TYPE I PROTON-TRANSLOCATING PYROPHOSPHATASE* is downregulated 2-fold and 3-fold at midday of days 9 and 12.

During the day, malic acid is released from the vacuole and, depending on the species, is believed to be decarboxylated by NADP-ME, NAD-ME, and/or PEP CARBOXYKINASE (PEPCK; Dittrich, 1976). In *T. triangulare*, the plastidial *NADP-ME4* was upregulated 5-fold at midday to 780 rpm and the apparent cytosolic *NADP-ME1* was upregulated 6-fold to 579 rpm, while

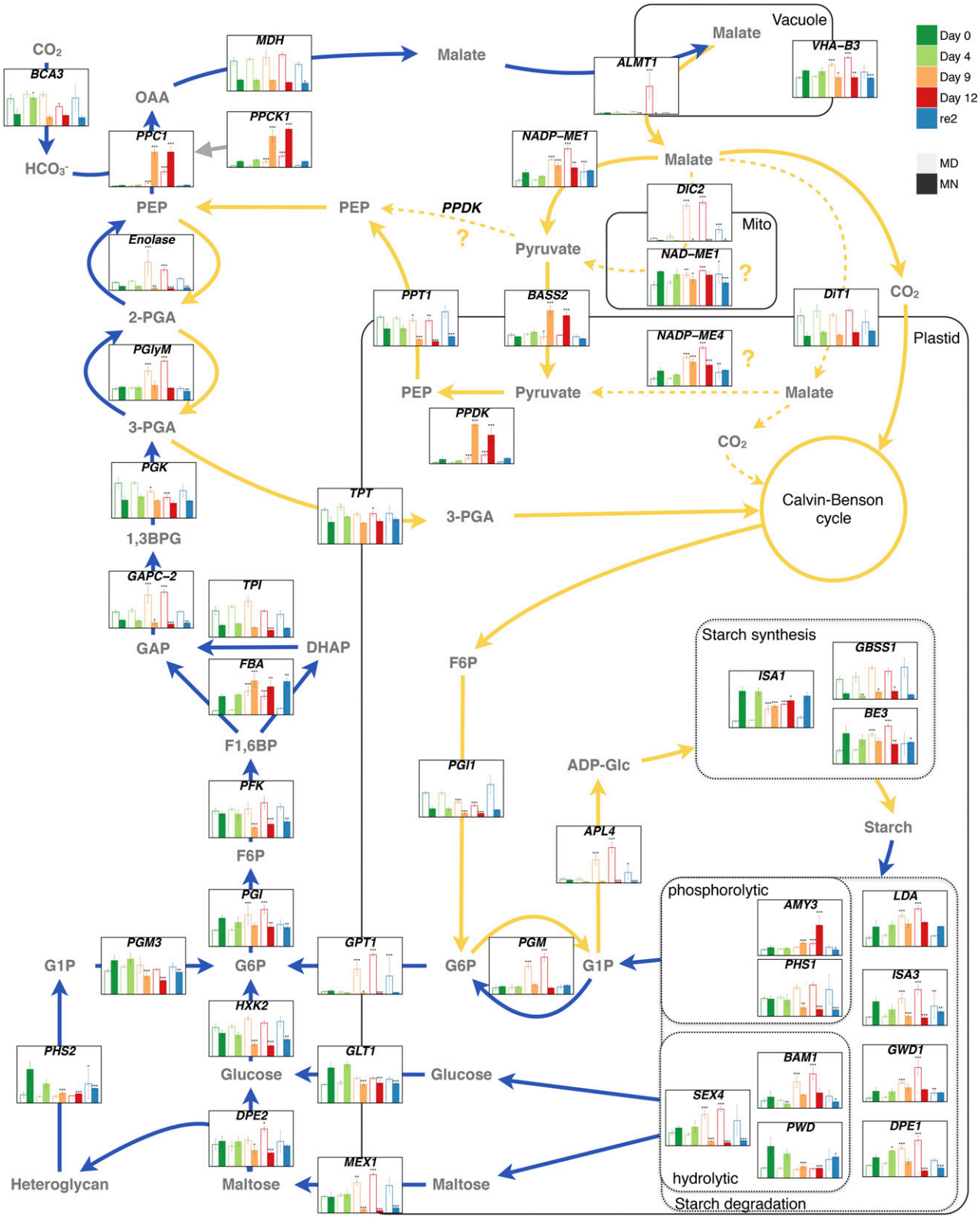

Figure 3. Abundances of CAM genes sensu stricto and sensu lato. Scheme of carbon assimilation via CAM and gene expression of central enzymes and transporters. Metabolites are represented in gray. Transcript levels were measured at the middle of the day and the middle of the night in leaves of *T. triangulare* plants under five different stages of water availability. Scaled to largest expression by gene; mean ± SD, $n = 3$. Asterisks indicate differential gene expression in comparison to day 0 as determined by

NAD-ME1 was 2-fold upregulated to 173 rpm and *PEPCK* was not significantly upregulated. The *T. triangulare* contigs of NADP-ME extracted from the assembly with high-read mappings possess a target peptide and cluster with the plastidial AtNADP-ME4 with high bootstrap support (Supplemental Fig. S3; Supplemental Table S5). In contrast to the downregulation of one isoform of *NADP-ME* at midnight in *M. crystallinum* (Cushman et al., 2008b), both genes encoding NADP-ME isoforms were upregulated at both midday and midnight on both CAM days. Transcript amounts of the plastidial DICARBOXYLATE TRANSPORTERS were unaltered (DiT1, expression between 256 and 381 rpm at midday, DiT2 between 48 and 105 rpm), while all three mitochondrial DICARBOXYLATE CARRIERS were upregulated at midday on both CAM days (DIC1 15-fold to 787 rpm, DIC2 12-fold to 899 rpm, DIC3 14-fold to 310 rpm on day 12). The plastidial pyruvate importer BILE-ACID SODIUM SYMPORTER2 (BASS2) was upregulated at night on both CAM days (4-fold to 411 rpm on day 9). Pyruvate, produced by malate decarboxylation, is phosphorylated to PEP by PPDK encoded by a single gene (9-fold upregulated to 18,371 rpm at midnight on day 9) and fed back to gluconeogenic starch synthesis (Kluge and Osmond, 1971). Extraction, alignment, and quantification of two different contigs encoding for PPDK (Supplemental Table S6) revealed markedly increased transcript amounts during CAM exclusively for one contig, Tt26901, which encodes for a protein with a 77 amino acid shorter N terminus. At midnight on day 12 transcript amounts for Tt26901 were 59-fold higher than for the longer PPDK encoding contig Tt24575 (Supplemental Table S6). Transcript amounts of the PEP/PHOSPHATE TRANSLOCATOR (PPT), catalyzing the export of PEP to the cytosol, were downregulated during CAM (4-fold to 23 rpm at midnight on day 12).

Another important aspect of CAM photosynthesis is starch turnover and its connection to the carboxylation/decarboxylation cycle. During the night, starch is degraded, likely both via the phosphorolytic and hydrolytic pathways, to provide PEP for PEPC via glycolysis (Weise et al., 2011). Four genes encoding enzymes, required both for phosphorolytic and hydrolytic starch degradation according to Weise et al. (2011) and Streb and Zeeman (2012), LIMIT DEXTRINASE (LDA), ISOAMYLASE3 (ISA3), GLUCAN WATER DIKINASE (GWD1), and DISPROPORTIONATING ENZYME1 (DPE1), were upregulated at midday on both CAM days (e.g. on day 12: 4-fold to 178 rpm, 4-fold to 195 rpm, 10-fold to 995 rpm and 3-fold to 197 rpm, respectively). *ISA3* is downregulated 3-fold at midnight on both CAM days and *DPE1* is downregulated at midnight of day 12. Genes encoding enzymes specific for hydrolytic starch degradation, PHOSPHOGLUCAN PHOSPHATASE (abbreviated SEX4 for STARCH EXCESS4) and BETA-AMYLASE1 (BAM1) were upregulated at midday (5-fold to 863 rpm and 3-fold to 150 rpm, respectively) as well, while the gene encoding PHOSPHOGLUCAN, WATER DIKINASE (PWD) was downregulated at midnight on both CAM days. Of the two exporters, MALTOSE EXPORTER1 (MEX1) and PLASTIDIC GLC TRANSLOCATOR1 (GLT1) exporting the hydrolytic breakdown products maltose and Glc (Weber et al., 2000; Niittylä et al., 2004), only the gene encoding MEX1 was significantly upregulated 2-fold on both CAM days at midday. MEX1 and GLT1 were both downregulated at midnight on both CAM days. The cytosolic enzymes catalyzing the conversion of Glc and maltose to Glc-phosphates (HEXOKINASE2 [HXK2], DPE2, STARCH PHOSPHORYLASE2 [PHS2] and PHOSPHOGLUCOMUTASE3 [PGM3]) were all downregulated at midnight upon drought (e.g. on day 12: 2-fold to 78 rpm, 2-fold to 110 rpm and 3-fold to 111 rpm, respectively). Of the enzymes specific for phosphorolytic starch degradation, the gene encoding ALPHA-AMYLASE3 (AMY3) was upregulated (4-fold on day 12 to 702 rpm), while the plastidial PHS1 gene was downregulated (3-fold on day 12 to 252 rpm) at midnight on both CAM days. The Glc-6-phosphate (G6P) exporter (*GPT*) expression was highly induced at midday upon CAM induction (17-fold; 1,095 rpm on day 12) and downregulated at midnight on day 12 (5-fold to 20 rpm).

The genes encoding cytosolic glycolytic enzymes PHOSPHOGLUCOSE ISOMERASE (PGI, upregulated 2-fold to 171 rpm at midday), PHOSPHOFRUCTOKINASE (PFK, constitutive level at midday ranging from 275 to 361 rpm), FRU-BISPHOPHATE ALDOLASE (FBA, upregulated 5-fold at midday on day 12 to 1,247 rpm), TRIOSEPHOSPHATE ISOMERASE (TPI, constitutive level at midday ranging from 980 to 1,541 rpm), SUBUNIT C2 OF GLYCERALDEHYDE-3-PHOSPHATE DEHYDROGENASE (GAPC-2, upregulated 2-fold at midday to 2,649 rpm), PHOSPHOGLYCERATE MUTASE (PGlyM, upregulated at midday 4-fold to 675 rpm), and ENOLASE (upregulated 3-fold to 2,273 rpm) were of high abundance or more abundant in CAM at midday. The gene encoding PHOSPHOGLYCERATE MUTASE (PGK) is of lower abundance (2-fold at midday to 1,167 rpm on day 12). The glycolytic enzymes, whose transcripts

Figure 3. (*Continued.*)
DESeq2, * $q < 0.05$, ** $q < 0.01$, and *** $q < 0.001$. Blue and yellow arrows represent reactions occurring at night and day, respectively. Abbreviations are explained in the text and in Supplemental Dataset S3. Question mark and dotted arrows indicate putative activity of plastidial NADP-ME, mitochondrial NAD-ME, and cytosolic PPDK as discussed in the text. Separation into phosphorolytic and hydrolytic starch degradation is based on the models presented by Weise et al. (2011) and Streb and Zeeman (2012). 1,3-BPG, 1,3-Bisphosphoglycerate; 2-PGA, 2-phosphoglycerate; 3-PGA, 3-phosphoglycerate; DHAP, dihydroxyacetone phosphate; F1,6BP, Fru 1,6-bisphosphate; F6P, Fru 6-phosphate; G1P, Glc 1-phosphate; G6P, Glc 6-phosphate; GAP, glyceraldehyde 3-phosphate; Mito, mitochondrion; re2, 2 d after rewatering.

were more abundant, produce 3-phosphoglycerate (3-PGA), which may enter the chloroplast via TRIOSE PHOSPHATE/PHOSPHATE TRANSLOCATOR (TPT, constitutive level ranging from 1,632 to 2,905 rpm). Triose-phosphates (3-PGA and GAP) resulting from Rubisco-based carbon fixation and from recycling the pyruvate out of the decarboxylation reaction can be stored as starch. The genes encoding starch precursor biosynthetic enzymes, PHOSPHOGLUCOMUTASE (PGM) and the LARGE SUBUNIT 4 OF ADP-GLC PYROPHOSPHORYLASE (APL4), were more abundant (6-fold to 1063 rpm and 9-fold to 3790 rpm at midday on day 12, respectively) and transcript levels of the GRANULE-BOUND STARCH SYNTHASES (GBSS) were unchanged while those of ISA1 and STARCH BRANCHING ENZYME3 (BE3) were significantly less abundant (4-fold to 66 rpm and 3-fold to 296 rpm at midday, respectively). The transcript levels of more abundant genes involved in carboxylation, decarboxylation, glycolysis, and gluconeogenesis were reduced to the levels of well-watered plants upon rewatering, except for *GWD* (3-fold upregulated at midday), *GPT1* (4-fold upregulated at midday), and *NADP-ME1* (3-fold upregulated at midday), which remained highly abundant on day 2 after rewatering.

Malate, Citrate, Soluble Sugars, and Starch

In C_3 performing plants, malate levels were somewhat higher at midday than at midnight (Fig. 4, day 0, 4, and 2 d after rewatering). By contrast, in plants exhibiting CAM (Fig. 4, days 9 and 12; Supplemental Table S2), malate levels were up to 8-fold higher at midnight as compared to midday and up to 4-fold higher as compared to midnight during C_3. The increased malate levels at midnight are consistent with the increased acidification measured at the end of the night (Fig. 1B) but did not reflect the full diurnal amplitude during the light/dark cycle. As midnight levels are higher than midday levels, malate decarboxylation may occur quite rapidly during the first 6 h of the light period (Fig. 4). Citrate showed a similar pattern to malate, as observed in other CAM species (Winter and Smith, 1996; Lüttge, 2002), with increased amounts during the night in CAM plants compared to C_3 plants, albeit with a lower amplitude than malate. In agreement with the C_3 plant Arabidopsis (Smith et al., 2004), *T. triangulare* leaves performing C_3 photosynthesis showed high Glc, Fru, and Suc pool sizes at the middle of the day, reflecting high photosynthetic activity (Fig. 4). While Glc and Fru levels dropped at night, Suc levels in the middle of the night were high, probably due to Suc synthesis from starch during the night as reported previously (Chia et al., 2004; Smith et al., 2004). The amounts of Glc, Fru, and Suc during the day and night dropped in CAM conditions (days 9 and 12) and were accompanied by reduced amounts of starch. The total amount of starch showed a continuous decrease from days 4 to 9 to 12. Two days after rewatering, starch levels were increased to the amounts before drought, while Glc, Fru, and Suc pools were not fully restored.

The photorespiratory metabolites glycerate and glycolate were significantly reduced in CAM conditions (Supplemental Fig. S4). During the day, glycerate was depleted 40.2-fold and 238.9-fold on days 9 and 12, and during the night, 3.6-fold and 16.7-fold. Glycolate was depleted during the day on days 9 and 12 (2.2-fold and 3.1-fold).

The contents of the putative compatible solute raffinose increased significantly during day (14.4-fold and 12.3-fold) and night (9.2-fold and 4.7 fold) on days 9 and 12 compared to day 0, and the increased amounts at night were not fully reverted 2 d after rewatering (Fig. 4). Well-known compatible solutes in C_3 plants (Bohnert et al,, 1995; Hare et al., 1998), Pro and the sugar alcohol

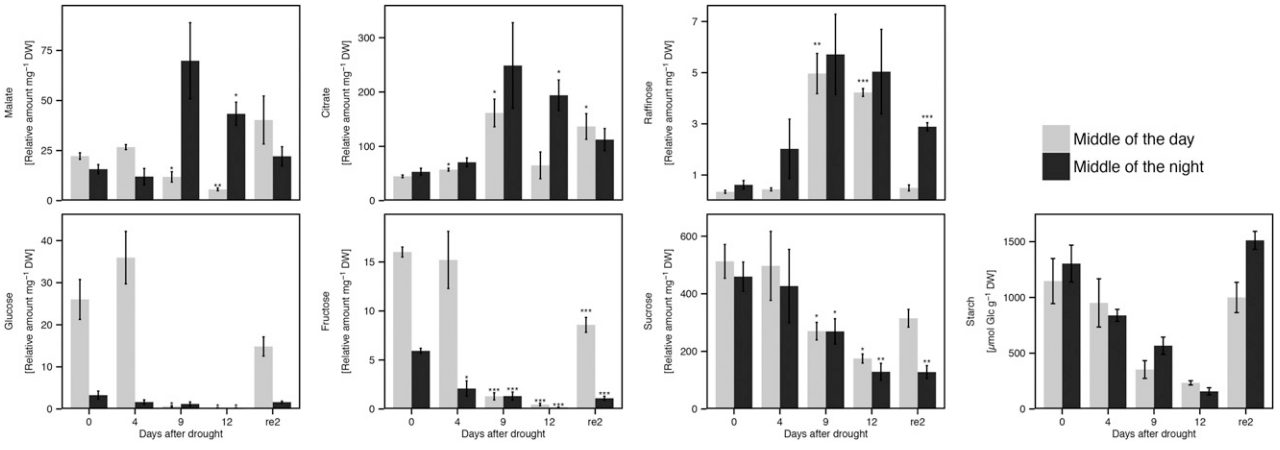

Figure 4. Levels of organic acids, soluble sugars and starch in *T. triangulare* in response to varying levels of water availability. Except for starch, all metabolites were measured by GC-MS and normalized to dry weight (DW) and internal ribitol standard (mean ± SE, $n = 3$–4, asterisks indicate Student's *t* test significance in comparison to day 0 at $^{***}P < 0.001$, $^{**}P < 0.01$, and $^{*}P < 0.05$). Starch was normalized to dry weight (mean ± SE, $n = 2$–4). re2, 2 d after rewatering.

mannitol, were only enriched in individual plants of the biological replicates (Supplemental Fig. S5).

Mapman and *K*-Means Clustering Indicate Multiple Layers of Response and Regulation

In order to understand alterations of mRNA amounts beyond the changes in the CAM-related genes described earlier (Fig. 3), three independent analyses were used to test general changes at the metabolic pathway and single gene level: (1) Mapman-based analysis using all values followed by Wilcoxon Rank Sum test (see "Materials and Methods") for enrichment (Thimm et al., 2004; Supplemental Fig. S6), (2) *k*-means clustering of the significantly changed genes followed by gene ontology (GO) term enrichment analysis (Fig. 5), and (3) manual inspection of the 50 genes with the highest fold changes on day 12 (Tables I and II). In Mapman (Supplemental Fig. S6), the metabolism overview again indicated little to no gene expression changes on day 4 of drought and rewatered plants compared to well-watered samples and massive changes during days 9 and 12 of water-limitation (Supplemental Fig. S6). The changes included downregulation of genes involved in cell wall metabolism (Supplemental Dataset S4). Genes of cell wall proteins of all classes were markedly downregulated ($q < 10^{-6}$ at midday), as were the biosynthesis genes for cell wall polymers (cellulose: $q < 10^{-08}$; modifiers: $q < 10^{-10}$ at midday; pectin esterases: $q < 10^{-11}$; pectate lyase: $q < 10^{-11}$, precursor synthesis: $q < 10^{-7}$; hemicellulose: $q < 10^{-6}$ at midnight). Downregulation of photosynthetic genes of the light reactions was visible on day 9 but more pronounced on day 12 of drought ($q < 10^{-5}$). Consistent with the previous analysis (Fig. 3), starch turnover genes ($q < 10^{-4}$) and genes of glycolysis ($q < 10^{-3}$ on day 12) were strongly upregulated. Additional strong upregulation was limited to the genes in the raffinose synthesis pathway ($q < 10^{-2}$), the committed step of Pro biosynthesis, and to the myoinositol oxidases (Tables I and II).

K-means clustering grouped 6,800 significantly DEGs at midday compared to day 0 by transcriptional pattern into 12 clusters (Fig. 5). Six clusters contained 3,124 genes ascending (clusters 1–6, Fig. 5), and six clusters contained 3,676 genes descending with pronounced water-limitation (7–12, Fig. 5). The clusters with ascending genes included one cluster with gradual increase up to day 12 and only little recovery after 2 d of rewatering (cluster 1). This cluster was enriched in GO terms related to external stimulus, and response. clusters 2 and 3 show mostly stable expression between days 9 and 12 and the expression was fully (cluster 2) and partially (cluster 3) recovered upon 2 d of rewatering. The list of genes with fully restored abundance of cluster 2 is enriched in GO terms related to chloroplast organization, protein localization, and starch. The genes in cluster 3 recovered only partially to well-watered levels after rewatering, and this cluster showed significant enrichment of terms related to

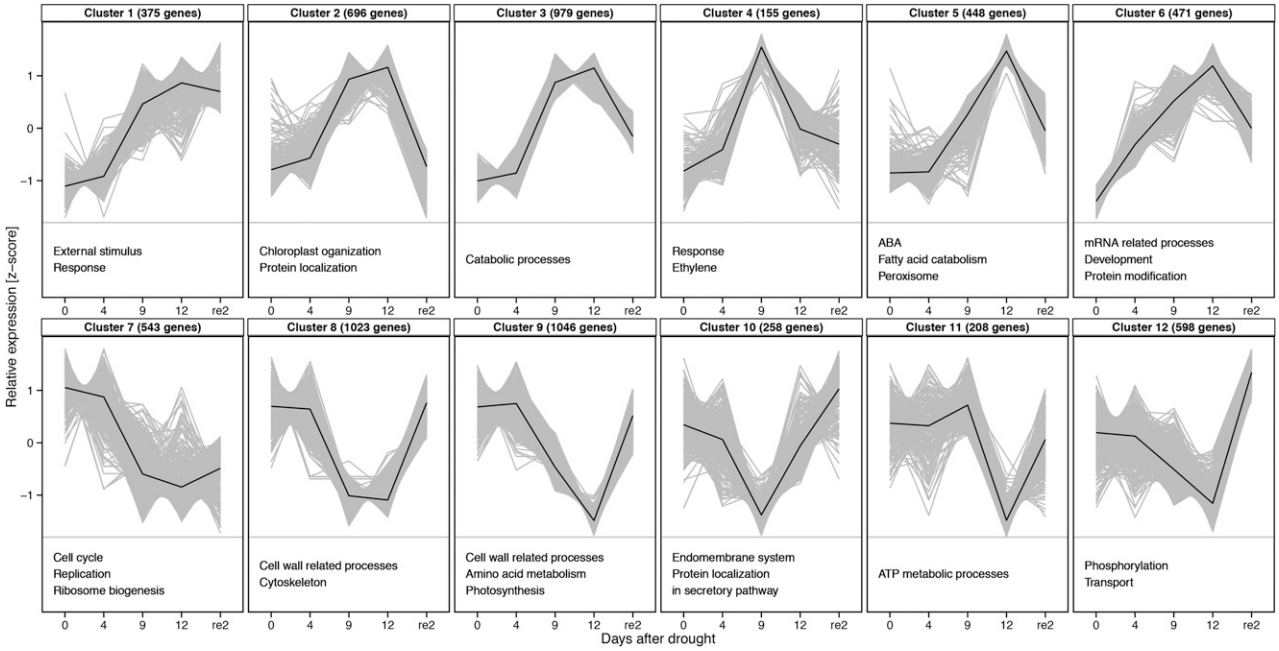

Figure 5. *K*-means clustering of relative gene expression and selected enriched GO terms. Genes that were found to be differentially expressed in the middle of the day between one of the water-limited stages and day 0 (DESeq2, $q < 0.01$) were used for the *k*-means approach (6800 genes in total). For the full list of enriched GO terms, see Supplemental Dataset S4. Gray line, Expression of single genes; black line, average of all genes in cluster; re2, 2 d after rewatering.

Table I. *Fifty most highly upregulated genes on day 12 after drought*

rpm, Reads per million ($n = 3$); MD, middle of the day; MN, middle of the night; log_2-FC, log_2-fold change in expression at given time point on day 12 compared to day 0; ns, not significantly DEG.

Locus	Annotation (TAIR10)	Day 0 MD	Day 0 MN	Day 12 MD	Day 12 MN	Log_2-FC (MD ; MN)
		rpm	*rpm*	*rpm*	*rpm*	
AT2G42600	Phospho*enol*pyruvate carboxylase 2	208.67	374.33	4,803.67	9,910.67	4.05 ; 4.7
AT1G53310	Phospho*enol*pyruvate carboxylase 1	312.00	613.33	6,656.33	15,510.33	3.91 ; 4.61
AT4G17030	Expansin-like B1	0.00	0.00	4.67	1.67	4.91 ; 2.55
AT4G26260	Myoinositol oxygenase 4	1.00	0.00	373.33	29.00	7.36 ; 5.02
AT1G14520	Myoinositol oxygenase 1	3.33	1.33	1,290.00	112.67	7.25 ; 5.42
AT2G19800	Myoinositol oxygenase 2	1.67	0.67	451.00	37.00	6.6 ; 4.83
AT1G55740	Seed imbibition 1	9.33	46.67	605.33	2,236.33	5.41 ; 5.38
AT3G08860	PYRIMIDINE 4	3.33	44.33	139.67	23.33	4.68 ; ns
AT2G38400	Ala:glyoxylate aminotransferase 3	2.67	30.00	103.67	17.67	4.54 ; ns
AT3G50980	Dehydrin xero 1	0.00	0.00	7.67	0.00	4.9 ; ns
AT3G22840	Chlorophyll A-B binding family protein	17.67	15.00	4,029.67	17.33	6.74 ; ns
AT5G15250	FTSH protease 6	6.67	2.67	764.33	3.00	6.18 ; ns
AT5G20110	Dynein light chain type 1 family protein	3.67	23.67	368.67	12.33	6.05 ; ns
AT4G27360	Dynein light chain type 1 family protein	19.67	32.33	654.33	54.33	4.62 ; 0.83
AT3G29410	Terpenoid cyclases/Protein prenyltransferases superfamily protein	0.00	0.00	4.67	17.67	4.86 ; 5.96
AT5G16020	Gamete-expressed 3	0.33	1.33	41.00	3.67	5.75 ; 1.59
AT1G80920	Chaperone DnaJ-domain superfamily protein	0.33	12.33	23.33	578.33	4.6 ; 5.46
AT3G22740	Homo-Cys S-methyltransferase 3	2.33	23.33	118.33	145.33	5.08 ; 2.68
AT1G10060	Branched-chain amino acid transaminase 1	1.00	4.67	31.33	11.00	4.63 ; ns
AT1G29900	Carbamoyl phosphate synthetase B	69.67	80.67	309.67	1,955.67	1.75 ; 4.56
AT1G12740	Cytochrome P450, family 87, subfamily A, polypeptide 2	4.00	86.33	290.67	10.67	4.47 ; -2.13
AT1G52240	RHO guanyl-nucleotide exchange factor 11	6.67	113.33	1,652.00	31.00	7.23 ; -1.69
AT1G28480	Thioredoxin superfamily protein	1.00	0.67	2.00	37.00	ns ; 5.76
AT1G18100	PEBP (phosphatidylethanolamine-binding protein) family protein	1.00	1.00	34.67	59.00	4.52 ; 5.57
AT1G03790	SOMNUS	0.00	0.67	19.67	4.33	5.15 ; 2.38
AT1G54070	Dormancy/auxin associated family protein	0.00	1.67	2.33	75.33	2.5 ; 5.01
AT1G80390	Indole-3-acetic acid inducible 15	0.00	0.00	5.67	5.33	4.73 ; 5
AT5G12840	Nuclear factor Y, subunit A1	0.67	2.67	25.67	31.00	4.75 ; 3.56
AT1G15330	Cystathionine beta-synthase (CBS) protein	0.00	0.00	1.33	5.00	3.54 ; 4.74
AT3G21700	Ras-related small GTP-binding family protein	0.67	3.00	17.33	82.33	3.56 ; 4.61
AT1G21000	PLATZ transcription factor family protein	0.33	25.33	18.33	135.00	4.48 ; 2.45
AT3G63060	EID1-like 3	0.00	0.00	22.00	13.33	5.88 ; 5.32
AT3G48530	SNF1-related protein kinase regulatory subunit gamma 1	0.67	31.00	39.67	275.00	5.05 ; 3.1
AT5G56550	Oxidative stress 3	1.33	4.33	18.33	310.33	3.03 ; 5.71
AT5G47560	Tonoplast dicarboxylate transporter	0.00	0.00	5.33	10.67	4.99 ; 5.93
AT1G32450	Nitrate transporter 1.5	4.33	68.00	233.67	34.33	5.04 ; ns
AT4G21680	NITRATE TRANSPORTER 1.8	2.00	20.33	101.33	16.67	5.02 ; ns
AT3G27250	Unknown	0.00	1.00	85.67	58.33	7.08 ; 5.63
AT1G52720	Unknown	0.67	26.67	156.33	80.33	6.72 ; 1.63
AT4G19390	Uncharacterized protein family (UPF0114)	6.33	49.33	1,234.33	276.00	6.58 ; 2.35
AT3G03170	Unknown	0.00	0.67	4.33	66.00	3.56 ; 6.21
AT3G48510	Unknown	2.67	1.33	78.33	106.00	4.16 ; 6.08
AT4G26288	Unknown	0.00	0.33	2.00	32.67	3.02 ; 5.99
AT5G40790	Unknown	1.67	0.33	38.33	48.00	3.96 ; 5.85
AT1G15380	Lactoylglutathione lyase/glyoxalase I family protein	4.67	9.67	337.00	109.33	5.65 ; 3.42
AT5G50360	Unknown	1.00	0.00	3.67	11.67	ns ; 5.3
AT2G44670	Protein of unknown function (DUF581)	0.33	2.33	3.33	65.67	1.92 ; 4.81
AT5G02020	Unknown	1.67	3.33	7.33	96.67	1.74 ; 4.57
AT1G27461	Unknown	0.00	0.00	0.00	3.67	ns ; 4.51
AT2G28780	Unknown	0.33	0.00	16.00	0.00	4.49 ; ns

Table II. *Fifty most highly downregulated genes on day 12 after drought*

rpm, Reads per million ($n = 3$); MD, middle of the day; MN, middle of the night; log_2-FC, log_2-fold change in expression at given time point on day 12 compared to day 0; ns, not significantly DEG.

Locus	Annotation (TAIR10)	Day 0 MD	Day 0 MN	Day 12 MD	Day 12 MN	Log_2-FC (MD ; MN)
		rpm	*rpm*	*rpm*	*rpm*	
AT5G20630	Germin 3	2,449.67	648.33	2.00	1.67	−9.13 ; −7.24
AT1G72610	Germin-like protein 1	932.67	274.67	1.00	1.00	−8.55 ; −6.45
AT1G64390	Glycosyl hydrolase 9C2	177.00	80.00	0.67	1.67	−7.45 ; −5.27
AT4G21960	Peroxidase superfamily protein	1,529.33	8,040.00	10.67	349.67	−7.09 ; −4.22
AT4G11050	Glycosyl hydrolase 9C3	70.67	31.67	0.00	0.33	−7.06 ; −5.32
AT5G22740	Cellulose synthase-like A02	272.67	207.00	3.33	4.67	−6.42 ; −5.27
AT2G32990	Glycosyl hydrolase 9B8	42.00	34.33	0.33	0.00	−6.36 ; −6.19
AT2G04780	FASCICLIN-like arabinoogalactan 7	15.00	24.33	0.00	0.00	−6.12 ; −6.27
AT4G37450	Arabinogalactan protein 18	10.33	22.67	0.00	0.00	−5.64 ; −6.24
AT2G35860	FASCICLIN-like arabinogalactan protein 16 precursor	94.33	125.67	2.67	1.33	−5.11 ; −6.12
AT5G03760	Nucleotide-diphospho-sugar transferases superfamily protein	61.00	64.33	1.00	0.67	−5.75 ; −6.11
AT2G37130	Peroxidase superfamily protein	21.00	7.67	0.00	0.00	−6.03 ; −4.26
AT3G11700	FASCICLIN-like arabinogalactan protein 18 precursor	129.33	195.67	4.67	2.67	−5.04 ; −5.92
AT1G02335	germin-like protein subfamily 2 member 2 precursor	9.33	16.33	0.00	0.00	−5.47 ; −5.91
AT1G67750	Pectate lyase family protein	15.00	53.33	0.00	0.67	−5.82 ; −5.5
AT4G13410	Nucleotide-diphospho-sugar transferases superfamily protein	27.67	23.00	0.67	0.00	−5.65 ; −5.81
AT3G28150	TRICHOME BIREFRINGENCE-LIKE 22	35.67	12.00	0.33	0.00	−5.79 ; −5.33
AT3G53190	Pectin lyase-like superfamily protein	14.67	23.33	0.00	1.00	−5.79 ; −4.07
AT3G62020	Germin-like protein 10	8.33	14.33	0.00	0.00	−5.66 ; −5.65
AT1G12090	Extensin-like protein	151.33	29.33	3.33	1.33	−5.65 ; −4.22
AT1G41830	SKU5-similar 6	19.00	47.33	0.33	0.33	−5.03 ; −5.65
AT5G46890	Bifunctional inhibitor/lipid-transfer protein/seed storage 2S albumin superfamily protein	28.67	5.67	0.00	0.00	−6.42 ; −3.84
AT3G04290	Li-tolerant lipase 1	235.00	817.67	1.00	13.00	−6.39 ; −4.91
AT1G76160	SKU5 similar 5	37.33	89.33	0.33	1.00	−6.13 ; −6.34
AT5G33370	GDSL-like Lipase/Acylhydrolase superfamily protein	162.00	675.00	1.00	6.33	−6.17 ; −5.57
AT5G23940	HXXXD-type acyl-transferase family protein	95.00	148.33	1.33	11.67	−6.13 ; −3.47
AT3G16370	GDSL-like Lipase/Acylhydrolase superfamily protein	298.00	307.67	5.33	4.67	−5.98 ; −5.78
AT3G15850	Fatty acid desaturase 5	20.00	9.00	0.00	2.00	−5.91 ; −1.93
AT1G21850	SKU5 similar 8	17.33	35.33	0.33	0.67	−5.17 ; −5.73
AT4G28780	GDSL-like Lipase/Acylhydrolase superfamily protein	111.00	569.33	0.33	4.33	−5.63 ; −5.47
AT1G63710	Cytochrome P450, family 86, subfamily A, polypeptide 7	45.00	193.33	1.00	1.00	−5.27 ; −6.59
AT3G10185	Gibberellin-regulated family protein	177.33	292.33	1.00	4.33	−6.46 ; −4.94
AT1G12570	Glc-methanol-choline (GMC) oxidoreductase family protein	88.67	59.33	1.00	2.67	−6.09 ; −4.2
AT2G45970	Cytochrome P450, family 86, subfamily A, polypeptide 8	34.33	140.33	1.00	1.33	−5.3 ; −6.07
AT1G74670	Gibberellin-regulated family protein	19.67	28.00	0.00	0.33	−6.03 ; −5.03
AT1G61720	NAD(P)-binding Rossmann-fold superfamily protein	6.00	89.67	0.00	0.67	−3.32 ; −5.82
AT3G52500	Eukaryotic aspartyl protease family protein	43.33	35.67	1.33	0.33	−5.01 ; −5.75
AT5G44635	Minichromosome maintenance (MCM2/3/5) family protein	37.67	6.67	0.00	0.00	−6.6 ; −4.12
AT5G67100	DNA-directed DNA polymerases	21.67	9.67	0.33	1.00	−5.93 ; −3.47
AT5G46280	Minichromosome maintenance (MCM2/3/5) family protein	26.67	5.33	0.00	0.00	−5.91 ; −3.97
AT1G44900	minichromosome maintenance (MCM2/3/5) family protein	66.00	12.00	0.67	0.33	−5.87 ; −3.62
AT2G07690	Minichromosome maintenance (MCM2/3/5) family protein	73.67	22.67	1.33	5.67	−5.74 ; −1.74
AT4G02060	Minichromosome maintenance (MCM2/3/5) family protein	38.00	6.33	0.67	0.00	−5.73 ; −3.52
AT1G27040	Major facilitator superfamily protein	44.33	2.67	0.00	2.00	−6.87 ; ns
AT5G62730	Major facilitator superfamily protein	40.00	3.00	0.00	3.00	−6.49 ; ns
AT3G02500	Unknown	28.33	4.00	0.33	0.00	−5.89 ; −3.27
AT1G27930	Protein of unknown function (DUF579)	8.67	19.00	0.00	0.00	−4.65 ; −5.79
AT2G21100	Disease resistance-responsive (dirigent-like protein) family protein	16.33	49.67	0.67	0.33	−4.04 ; −5.66
AT4G17340	Tonoplast intrinsic protein 2;2	321.33	125.00	3.67	31.00	−5.74 ; ns
AT1G13260	Related to ABI3/VP1 1	18.33	5.33	0.00	0.33	−5.86 ; −3.45

catabolic processes. Cluster 4 was only transiently upregulated on day 9 of water withholding but dropped back to background levels on day 12. It was enriched with GO terms relating to responses to signals, which include ethylene and mechanical stimulus. The expression of genes in clusters 5 and 6 peaked on day 12. Genes of cluster 5 only responded after 9 d of drought, increased sharply toward day 12, and mostly recovered after 2 d of rewatering and were enriched in GO terms related to ABA, fatty acid catabolism, and peroxisomes. The expression of genes in cluster 6 responded already after 4 d of drought, was only partially reverted and was enriched for mRNA related processes, development, and protein modification.

Similar to cluster 1, where genes were upregulated and stayed mostly up despite rewatering, cluster 7 contained genes that dropped in expression during days 9 and 12 of drought and barely recovered. Cluster 7 was enriched in genes related to growth, i.e. in GO terms referring to DNA replication, cell cycle, and ribosome genesis. Genes of cluster 8 were similarly downregulated during CAM conditions but fully recovered upon rewatering. This cluster is enriched in GO terms related to cell wall processes and cytoskeleton. Genes in cluster 9 only responded on day 9, further increased on day 12 of drought, and fully recovered after rewatering. This cluster was enriched in GO terms related to cell wall related processes, amino acid metabolism, and photosynthesis. Cluster 10 was the mirror cluster of cluster 4, which peaked on day 9, and included genes with peak downregulation on day 9. It was enriched in genes related to protein localization in the secretory pathway and the endomembrane system, including the protein population of the plasma membrane. Downregulation of genes in clusters 11 and 12 peaked on day 12. Genes in cluster 11 responded only after 12 d of drought and fully recovered after rewatering. This cluster was enriched in processes related to nucleotide metabolic processes. Expression of genes in cluster 12 began decreasing on day 4, continued to decrease until day 12, and after rewatering, were increased above well-watered levels. This overshoot cluster was enriched in genes related to posttranslational modification in particular phosphorylation and transport. Analogous *k*-means clustering of 7,563 significant DEGs at midnight revealed large overlap of major changes in comparison to day 0 at midday (Supplemental Fig. S7; Supplemental Dataset S5). Taken together, the clusters with elevated expression during drought mostly contained genes enriched in GO terms related to catabolism, RNA metabolism and also related to signaling. The clusters with reduced gene expression contained genes related to growth from photosynthesis over amino acid synthesis and cell wall processes to DNA replication and cell cycle.

To highlight the results of the analysis at the pathway level, the top 50 of significantly induced (Table I) and repressed (Table II) genes on day 12 of water limitation were analyzed. Of the fifty genes with the highest upregulation on day 12 in *T. triangulare*, 22 were upregulated by ABA in Arabidopsis (Table I). The CAM gene *PPC* was among the top fifty upregulated genes. Six genes were related to production of compatible solutes or their precursors including raffinose, beta-Ala, and sugar alcohols. One gene encoding a LATE EMBRYOGENESIS ABUNDANT (LEA) protein was among the top 50 induced genes as well as a heat inducible chaperone and the oxidative stress responsive OXIDATIVE STRESS3 (OXS3). Light protection was seemingly strengthened as evidenced by EARLY LIGHT INDUCIBLE1 (ELIP1), FTSH PROTEASE6 (FTSH6), and two dyneins, which may be involved in organelle repositioning (Heddad and Adamska, 2000; Hutin et al., 2003; Zelisko et al., 2005). Proteins encoded by 11 of the 50 most induced genes were involved in regulation: the SNF1 RELATED KINASE REGULATORY SUBUNIT GAMMA1 (KING1), the F-box protein EID1-LIKE3 (EDL3), RHO GUANYL-NUCLEOTIDE EXCHANGE FACTOR11, and four transcription factors including SOMNUS and a PLATZ transcription factor. There were also three transport proteins affected.

The fifty genes most reduced in expression on day 12 included 21 genes involved in cell wall synthesis, nine genes related to lipid metabolism and the vacuolar aquaporin TONOPLAST INTRINSIC PROTEIN2;2 (Table II). Downregulation of DNA replication via downregulation of the genes (*MINICHROMOSOME MAINTENANCE2-3* and *5-7*) encoding five of six subunits of the helicase and downregulation of the gene encoding DNA-directed DNA polymerase INCURVATA2 was also evident among the fifty most downregulated genes, indicating cell-cycle arrest.

Mediators of the Transcriptional Changes

K-means clustering identified a multilayer response with genes only transiently regulated on day 9 of drought and with genes with sustained change on both day 9 and day 12 of drought. To identify the candidate transcriptional regulators mediating the responses, genes encoding for putative transcription factors were extracted from PlnTFDB (Pérez-Rodríguez et al., 2010) and tested for differential expression on either day 9 or day 12 of water limitation relative to the well-watered state (day 0) and for cluster membership. Of 1,449 identified transcription factor genes, 582 (40%) were differentially regulated on either day 9 or day 12 or both compared to well-watered plants (Supplemental Dataset S6). Of the 582, a subset of 19 transcription factor genes belonged to cluster 4, the genes, which were only transiently upregulated on day 9 of drought (Table III). These included eight TFs of the APETALA2 AND ETHYLENE-RESPONSIVE ELEMENT BINDING PROTEINS (AP2-EREBP) class including C-REPEAT/DRE BINDING FACTORS (CBF2 and CBF3), which are known to be stress induced (Zou et al., 2011), REDOX RESPONSIVE TRANSCRIPTION FACTOR1 (RRTF1) and ETHYLENE RESPONSE FACTOR8 (ERF8). Both CBFs were shown to bind the drought responsive

Table III. *Transcription factors of k-means cluster midday 4*

TF Family, Transcription factor family based on Pérez-Rodríguez et al. (2010).

Locus	Annotation (TAIR10)	TF Family
AT1G12610	Integrase-type DNA-binding superfamily protein	AP2-EREBP
AT1G19210	Integrase-type DNA-binding superfamily protein	AP2-EREBP
AT1G33760	Integrase-type DNA-binding superfamily protein	AP2-EREBP
AT1G53170	Ethylene response factor 8	AP2-EREBP
AT4G25470	C-repeat/DRE binding factor 2	AP2-EREBP
AT4G25480	Dehydration response element B1A	AP2-EREBP
AT4G34410	Redox responsive transcription factor 1	AP2-EREBP
AT5G21960	Integrase-type DNA-binding superfamily protein	AP2-EREBP
AT3G47640	Basic helix-loop-helix (bHLH) DNA-binding superfamily protein	bHLH
AT2G21230	Basic-Leu zipper (bZIP) transcription factor family protein	bZIP
AT1G27730	Salt tolerance zinc finger	C2H2
AT2G40140	SALT-INDUCIBLE ZINC FINGER 2	C3H
AT4G17230	SCARECROW-like 13	GRAS
AT1G18710	Myb domain protein 47	MYB
AT3G13540	Myb domain protein 5	MYB
AT1G01380	Homeodomain-like superfamily protein	MYB-related
AT1G33060	NAC 014	NAC
AT3G49530	NAC domain containing protein 62	NAC
AT4G35580	NAC transcription factor-like 9	NAC

element DNA sequence (Liu et al., 1998). Two zinc finger transcription factors, SALT TOLERANCE ZINC FINGER (STZ) and SALT-INDUCIBLE ZINC FINGER2 (SFZ2), belonged to cluster 4. STZ was shown to function as a transcriptional repressor in response to drought and ABA (Sakamoto et al., 2000, 2004), while SFZ2 is induced by salt stress (Sun et al., 2007). In addition, three genes encoding NO APICAL MERISTEM (NAC) domain proteins, one GRAS, one bZIP, and three MYB-domain proteins made up the transcriptional part of cluster 4. The known functions of transcription factors in the transient group indicated that *T. triangulare* underwent a transient general stress response commonly observed in plants mediated primarily by the drought responsive element binding transcription factors.

Of the remaining 563 genes encoding transcription factor candidates, the top 25 upregulated were analyzed for known functions (Table IV). The ABA-responsive proliferation inhibitor SOMNUS (SOM) was the most highly upregulated transcription factor on day 12. The top 25 also included four genes encoding transcription factors known to be involved in ABA signaling, NUCLEAR FACTOR Y, SUBUNIT A1 (NF-YA1), NF-YA9, and HOMEOBOX7 (HB7) and one NAC-like transcription factor, NAC-LIKE, ACTIVATED BY AP3/PI (NAP), which acts upstream of ABA biosynthesis and promotes chlorophyll degradation (Yang et al., 2014). In addition, two transcription factors of the Orphans family, ETHYLENE RESPONSE2 (ETR2) and ETHYLENE INSENSITIVE4 (EIN4), which were shown to antagonistically control seed germination under salt stress (Wilson et al., 2014) as well as three heat shock factor family proteins were among the 25 most upregulated transcription factors. The sustained response of *T. triangulare* included ABA responsive transcription factors and growth associated regulators, while the transient response included the DRE responsive TFs of the CBF family.

To test if phytohormones other than ABA are also involved in the drought response, the overlap between genes significantly changed on day 12 at midday and genes specifically altered by the application of different hormones in Arabidopsis (Goda et al., 2008) was determined and statistically evaluated. Among the genes shown to be upregulated during hormone treatment of Arabidopsis with ABA, auxin, brassinosteroids, cytokinine, and ethylene, only the ABA-upregulated genes were enriched among the *T. triangulare* drought-inducible genes (Supplemental Fig. S8). A total of 434 ABA-regulated genes of Arabidopsis were drought-induced genes in *T. triangulare* and, accordingly, 541 ABA-regulated genes of Arabidopsis were repressed by drought in *T. triangulare.* The ABA-, auxin-, brassinosteroid-, and ethylene-downregulated genes were enriched among the *T. triangulare* drought-repressed genes. However, only few genes were shown to be repressed by auxin, brassinosteroids, and ethylene (90, 11, and 23, respectively). Thus, among the phytohormones, ABA made the major contribution to the control of drought-controlled genes and likely controls at least one-fifth of the genes differentially regulated under drought conditions in *T. triangulare*.

To visualize the ABA contribution to changes in general metabolism, the Mapman map of ABA induced changes in Arabidopsis was compared with those occurring in *T. triangulare* (Supplemental Fig. S9). The map of ABA-responsive genes replicates the induction of raffinose synthesis genes, and a mild reduction of photosynthesis genes but failed to result in the major changes in cell wall synthesis and changed photorespiration, sulfur metabolism, and secondary metabolism. The ABA signal detected in Arabidopsis at the level of metabolic gene expression is not fully congruent with the signals detected in *T. triangulare*, indicating additional layers of regulation in *T. triangulare*.

DISCUSSION

Facultative CAM

During CAM induction in *T. triangulare*, several key components of the CAM-cycle sensu stricto were transcriptionally upregulated such as genes encoding

Table IV. *Twenty-five most highly upregulated transcription factors on day 12 after drought*

TF Family, Transcription factor family based on Pérez-Rodríguez et al. (2010); rpm, reads per million ($n = 3$); MD, middle of the day; MN, middle of the night; $\log_2$-FC, $\log_2$-fold change in expression at given time point on day 12 compared to day 0; ns, not significantly DEG.

Locus	Annotation (TAIR10)	TF Family	Day 0 MD	Day 0 MN	Day 12 MD	Day 12 MN	$\log_2$-FC (MD ; MN)
			rpm	*rpm*	*rpm*	*rpm*	
AT1G03790	SOMNUS	C3H	0.00	0.67	19.67	4.33	5.15 ; 2.38
AT5G12840	Nuclear factor Y, subunit A1	CCAAT	0.67	2.67	25.67	31.00	4.75 ; 3.56
AT1G21000	PLATZ transcription factor family protein	PLATZ	0.33	25.33	18.33	135.00	4.48 ; 2.45
AT3G54320	Integrase-type DNA-binding superfamily protein	AP2-EREBP	1.00	1.33	3.33	27.00	1.4 ; 4.41
AT5G67480	BTB and TAZ domain protein 4	TAZ	19.67	71.00	461.33	129.00	4.15 ; 0.95
AT2G46680	Homeobox 7	HB	7.67	38.00	165.33	445.00	3.92 ; 3.56
AT1G69490	NAC-like, activated by AP3/PI	NAC	8.67	76.00	206.33	366.00	3.73 ; 2.09
AT1G52880	NAC (No Apical Meristem) domain transcriptional regulator superfamily protein	NAC	0.00	2.67	5.00	10.67	3.51 ; 1.8
AT3G02550	LOB domain-containing protein 41	LOB	0.00	0.00	0.00	1.33	ns ; 3.3
AT1G17590	Nuclear factor Y, subunit A8	CCAAT	3.67	9.33	41.67	63.00	3.19 ; 2.75
AT3G23150	ETHYLENE RESPONSE 2	Orphans	12.33	10.67	86.00	94.00	2.47 ; 3.13
AT3G04580	ETHYLENE INSENSITIVE 4	Orphans	14.33	9.67	94.00	82.33	2.38 ; 3.13
AT2G26150	Heat shock transcription factor A2	HSF	4.67	6.00	9.00	47.00	ns ; 3.06
AT1G80840	WRKY DNA-binding protein 40	WRKY	2.33	0.67	0.33	6.67	−2.38 ; 3.04
AT4G17900	PLATZ transcription factor family protein	PLATZ	8.33	38.67	91.67	55.33	3.01 ; ns
AT3G11580	AP2/B3-like transcriptional factor family protein	ABI3VP1	0.33	1.33	4.33	1.67	3 ; ns
AT4G13980	Winged-helix DNA-binding transcription factor family protein	HSF	2.67	9.00	4.33	68.67	ns ; 2.98
AT3G24520	Heat shock transcription factor C1	HSF	2.67	11.33	5.00	88.00	ns ; 2.96
AT3G20910	Nuclear factor Y, subunit A9	CCAAT	11.00	25.67	72.67	181.00	2.32 ; 2.87
AT4G02640	bZIP transcription factor family protein	bZIP	1.67	6.67	0.67	48.33	ns ; 2.83
AT2G25900	Zinc finger C-x8-C-x5-C-x3-H type family protein	C3H	12.67	12.67	119.00	45.33	2.83 ; 1.91
AT3G15500	NAC domain containing protein 3	NAC	0.67	8.00	8.33	21.00	2.82 ; 1.39
AT1G32700	PLATZ transcription factor family protein	PLATZ	16.00	56.00	141.33	75.67	2.78 ; ns
AT4G39070	B-box zinc finger family protein	Orphans	1.00	3.00	1.67	22.00	ns ; 2.77
AT5G28770	bZIP transcription factor family protein	bZIP	2.67	11.00	2.00	74.00	ns ; 2.77

PEPC, NADP-ME, NAD-ME, and PPDK (Fig. 3). Other components, including transcripts of MDH and BCA3, remained unchanged but were constitutively highly expressed already prior to CAM induction. This is consistent with enzyme activity data for MDH (Holtum and Winter, 1982) and CA (Tsuzuki et al., 1982) in *M. crystallinum* operating in the C_3 and CAM modes, that were already very high in the C_3 state. Nonetheless, Cushman et al. (2008b) found additional upregulation of these enzymes during salt-induced CAM in *M. crystallinum*. In C_4 photosynthesis, activities of the corresponding carboxylation and decarboxylation enzymes required for CAM are not temporally but spatially separated into different cell types (Sage, 2003). In C_4 species of the genera *Flaveria* and *Cleome*, NAD-MDH is also not transcriptionally elevated relative to C_3 sister species (Bräutigam et al., 2011; Gowik et al., 2011) and CA only in some, but not in all, cases (Bräutigam et al., 2014).

In contrast to the canonical scheme of the CAM-cycle with NADP-ME localized in the cytosol (Holtum et al. 2005 and references therein), we found two isoforms of NADP-ME to be upregulated at both midday and midnight during CAM in the cross species mapping (Fig. 3; Supplemental Dataset S3). The contig analysis indicates that indeed two contigs are highly expressed; however, both possess a target peptide (Emanuelsson et al., 2000) and cluster with the plastidial AtNADP-ME4 with high bootstrap support. (Supplemental Fig. S3). The putative plastidic malate importers of the DiT family are not upregulated (Supplemental Dataset S3). NAD-ME was also upregulated, albeit at lower absolute levels but concomitant with the required malate importer DIC (Supplemental Dataset S3). Taken together, the data suggest that multiple routes for decarboxylation are possible. Unlike in the transcriptomic analyses of C_4 species (Bräutigam et al., 2011; Gowik et al., 2011), the transcriptomic evidence favors neither pathway in *T. triangulare*. It cannot be excluded that the low levels of CAM photosynthesis detected in *T. triangulare* (Winter and Holtum, 2014) are supported by multiple decarboxylation routes. Ideally our findings on the transcript levels of NAD(P)-ME would be confirmed by enzyme activity data, but so far all biochemical assays to measure activity in leaf material failed due to a suppression effect derived from an unknown constitute of the *T. triangulare* plant extract (Supplemental Fig. S10). Experimental differentiation

of the biochemical pathway of malate decarboxylation in the light during CAM in *T. triangulare* will be part of future work.

PPDK was strongly upregulated during CAM-induction in *T. triangulare* (Fig. 3). In *M. crystallinum*, the plastidic location of PPDK was demonstrated by measurements of enzyme acvitity combined with studies of pyruvate metabolism of intact isolated chloroplasts (Winter et al., 1982; Holtum et al., 2005). However, immunogold labeling of PPDK in the CAM species *Kalanchoë blossfeldiana* (Kondo et al., 2001) also raises the possibility of cytosolic PEP regeneration. In support of this hypothesis, the contig Tt26901, which encodes PPDK with a truncated N terminus, showed markedly higher transcript amounts on days 9 and 12 compared to day 0 and compared to the longer contig, which encodes for a putative target peptide. The contigs possibly represent splicing variants of the same gene and encode for PPDKs dually targeted to the cytosol (Tt26901, truncated N terminus) or the chloroplast (Tt24575) as found in Arabidopsis (Parsley and Hibberd, 2006). In C_4 species (NADP-ME and NAD-ME type), where the regeneration of PEP is invariably localized in the plastids, the transporters for pyruvate import (i.e. BASS2 and NHD1) and PEP export (i.e. PPT) are increased in expression compared to C_3 sister plants (Bräutigam et al., 2008, 2014; Furumoto et al., 2011). Interestingly, while BASS2 was upregulated but lowly expressed at midnight, transcripts encoding transporters of the PPT family were found to be downregulated during the C_3-CAM switch in *T. triangulare* (Supplemental Dataset S3). This contrasts with *M. crystallinum* where transcriptional induction of PPT was detected (Kore-eda et al., 2005). Transcripts matching the NHD1 gene were not detected. The absence of a target peptide in the major contig encoding for PPDK suggests that concomitant with the missing NHD1 and downregulated PPT, *T. triangulare* employs cytosolic PPDK. In addition to PPDK, both isoforms of PPDK regulatory protein, which promote circadian regulation of PPDK activity by dark-phased phosphorolytic inactivation (Dever et al., 2015), were slightly but significantly induced during CAM in *T. triangulare* (Supplemental Dataset S3).

During the evolution of C_4, the change of a single amino acid residue in the N-terminal region of PEPC, namely from Ala to Ser, was shown to increase the enzyme's kinetic efficiency compared to C_3 sister plants (Svensson et al., 1997; Bläsing et al., 2000; Svensson et al., 2003; Gowik et al., 2006). It was recently shown that in C_4 and CAM species within the *Caryophyllales*, to which the *Talinaceae* belong, the isogenes of a recurrently recruited gene lineage encoding PEPC1, namely *ppc1-E1c*, almost exclusively encodes the C_4-like Ser-780 (Christin et al., 2014). In the same study, in response to reduced irrigation, the expression of *ppc1-E1c* was upregulated at night in *Portulaca oleracea*, a C_4 species with facultative CAM (Christin et al., 2014). The two *PPC* contigs, Tt9871_4 and Tt9871_6, that exhibit the C_4-like Ser-780 (Supplemental Fig. S2A; Supplemental Table S3) indeed cluster together with *ppc1-E1c* isoforms of *Talinaceae* and *P. oleracea* (Supplemental Fig. S2B). However, highest transcript levels and the most drastic elevation in abundance during CAM induction was found for contig Tt63271, which encodes for the C_3-like Ala-780 and clusters in the *ppc1-E1b* clade. Low-level CAM photosynthesis apparently employs different PEPC genes compared to C_4 photosynthesis or fully expressed CAM photosynthesis. At night, PEPC is activated through phosphorylation via PEPC kinase (Carter et al., 1991), the activity of which is regulated transcriptionally through a circadian oscillator (Hartwell et al., 1996, 1999; Borland et al., 1999; Taybi et al., 2000). Phosphorylated PEPC is less sensitive to feedback inhibition by malate (Hartwell et al., 1996; Taybi et al., 2000, 2004). Consistent with the circadian regulation and strong upregulation of PEPC kinase at night during CAM induction in *M. crystallinum* (Hartwell et al., 1999; Cushman et al., 2008b; Dever et al., 2015), PEPC kinase was most markedly upregulated at midnight during CAM in *T. triangulare* (expression rank 300 on day 12, Supplemental Dataset S3), enabling increased PEPC activity at night. In contrast to C_4 plants, PEPC of CAM plants needs to be efficiently switched off during the light through feedback inhibition by malate exported from the vacuole to prevent futile cycling of CO_2 (Borland et al., 1999). All of the PEPC isoforms identified as upregulated in *Talinum* carry an Arg residue at position 890 (Supplemental Fig. S2; Supplemental Table S3; Paulus et al., 2013) and are thus likely feedback inhibited both by malate export during the day and once vacuolar storage capacity is exceeded during the night.

The upregulation of CAM-cycle genes was accompanied by elevated malate and citrate levels during the night and reduced malate levels during the day (Fig. 4) in agreement with increase in nocturnal acidity (Fig. 1). Photorespiration is not inactivated during the decarboxylation phase of CAM (Niewiadomska and Borland, 2007; Lüttge, 2011), and we observed a mostly stable expression of photorespiratory genes during the C_3-CAM transition (Supplemental Table S7). Reduced steady-state metabolite pools of glycerate and glycolate (Supplemental Fig. S4), as well as the reduced sugar levels, were likely a consequence of reduced overall photosynthetic rate. Nocturnal carbon assimilation rates during CAM were estimated to be reduced to approx. 5% of CO_2 fixation in the light in the C_3 mode (Winter and Holtum, 2014). Hence, the associated metabolite fluxes during CAM are expected to be low.

The carboxylation reaction during the night depends on degrading starch for PEP production. The degradation can be either phosphorolytic or hydrolytic (Häusler et al., 2000; Weise et al., 2011). Some, but not all, transcripts encoding these two alternate starch breakdown pathways were upregulated (Fig. 3). Phosphorolytic starch breakdown preserves some of the energy released during breakage of the glycosidic bonds in starch and therefore consumes less ATP for activation of the released Glc residues. ATP, ADP, and/

or free phosphate may balance hydrolytic and phosphorolytic starch breakdown depending on the ATP demand of the cytosol. Using starch and malate contents at the end of the night and the end of the day, the amount of starch turnover was calculated as sufficient to support the level of photosynthesis during CAM (Supplemental Table S8). Efficient starch turnover apparently required elevated expression of both starch synthesis and starch degradation genes, as well as sufficient branching of the starch to allow rapid degradation (Fig. 3). Based on strong upregulation of *GPT*, which was among the top 50 upregulated genes at midday, and the upregulation of *MEX1* (Fig. 3), glycolysis likely operated in the cytosol, which was confirmed by the transcriptional upregulation of all but one of the cytosolic glycolytic enzymes (Fig. 3). Taken together, inducible CAM required upregulation of key CAM-cycle genes, elevation of starch turnover by changes in selected genes and increased expression of cytosolic glycolytic genes. While starch turnover capacity is increased (Fig. 3), the amount of starch is reduced (Fig. 4), which may be explained by lowered photosynthetic capacity during CAM (Winter and Holtum, 2014). In contrast to *T. triangulare*, CAM can substantially contribute to carbon gain in *M. crystallinum* (Winter and Holtum, 2007), and following salinity-induced CAM, starch accumulation is increased and directly correlates with acidification (Haider et al., 2012).

The rapid induction of CAM-related gene expression and the coexpression of ABA-related signaling networks upon drought stress points to a direct connection to the ABA signaling network as shown for *Kalanchoë blossfeldiana* (Taybi et al., 1995) and *M. crystallinum* (Taybi and Cushman, 2002). Control of CAM induction may be exerted either directly by ABA-mediated phosphorylation and activation of transcription factors or by downstream effectors (Table IV).

Drought Response and Carbon Resource Utilization

Beyond CAM photosynthesis, additional processes contribute to the adaptation of *T. triangulare* to drought, such as a classical drought response and management of carbon resources. Water limitation leads to stomatal closure during the day (Herrera et al., 1991; Winter and Holtum, 2014), which reduces the photosynthetic carbon assimilation and hence pool sizes of soluble sugars such as Suc, Glc, and Fru during the day and the night (Fig. 4). Under severe drought stress, part of these remaining soluble sugars may act as compatible solutes, retain water in the cells and protect cellular structures against damage. In contrast to the overall loss of these sugars, substantial accumulation of raffinose was observed (Fig. 4) likely triggered by transcriptional upregulation of raffinose biosynthesis (Supplemental Fig. S6; Table I). During cold acclimation in Arabidopsis (Nägele and Heyer, 2013) and *Ajuga reptans* (Findling et al., 2015), nonaqueous fractionations localized raffinose to variable extents within the vacuole, cytosol and chloroplast stroma. At this point we do not know whether raffinose accumulating in drought-stressed *T. triangulare* functions as a compatible solute in the cytosol, supports osmotic pressure maintenance in the vacuole, or has protective functions for membranes and/or proteins within the plastid or cytosol (Nishizawa et al., 2008). Although the gene encoding PYRROLINE-5-CARBOXYLATE SYNTHASE (P5CS), which catalyzes the committed step for Pro synthesis, was upregulated during CAM (expression rank 57 on day 12 at midday, Supplemental Dataset S1), Pro accumulated only in some, but not all, plants tested (Supplemental Fig. S5). Similarly, levels of the sugar alcohols glycerol, mannitol, myoinositol, and sorbitol, which could potentially act as compatible solutes, were not significantly altered during drought, although mannitol accumulated in individual plants (Supplemental Figs. S5 and S11). The discrepancy between transcript and metabolite measurements is likely based on the fact that the transcriptome precedes the metabolome. Although genes were upregulated in all replicates (Supplemental Dataset S1), the metabolic status may be delayed.

Stomatal closure reduces the consumption of absorbed light energy in photosynthesis, potentially leading to short-term redox stress. Among the top 50 upregulated genes, four were involved in light stress, e.g. the gene of ELIP1 (Hutin et al., 2003), which is ABA induced in Arabidopsis (Table I). Genes encoding components of light stress-induced oxidation of fatty acids in the peroxisomes were enriched in cluster 3, representing induced genes that do not quite reach well-watered levels after rewatering (Fig. 5). Thus, despite leaf-angle changes and leaf rolling (Taisma and Herrera, 2003; Fig. 1) that reduce light exposure, a transcriptional upregulation of light-protection mechanisms is seemingly required to aid leaf functioning. Additionally, the increase of raffinose, shown to act as a scavenger of hydroxyl radicals in Arabidopsis (Nishizawa et al., 2008), might play a role in supporting leaf functioning.

Under drought, increased use of resources such as fatty acids and proteins was induced (Fig. 5), which might explain the slight increase in free amino acids (Noctor and Foyer, 2000; Supplemental Fig. S11). Catabolism of fatty acids through peroxisomal processes was induced by day 9 already, maintained on day 12, and only partially reversed upon rewatering. Genes involved in processes related to mRNA turnover were also increased during drought (Fig. 5, cluster 6). These induced catabolic processes were, however, not associated with permanent damage as the transcriptome returned to prestress status upon rewatering (Fig. 2). Most genes encoding anabolic processes such as photosynthesis and amino acid biosynthesis and transport were transcriptionally downregulated (Fig. 5; Supplemental Fig. S6), but returned to prestress levels after rewatering. For example, cell wall biosynthesis was downregulated and completely reversed upon rewatering (Fig. 5, clusters 8 and 9; Supplemental Fig. S6). Finally, genes involved in replication and the cell cycle were among the most downregulated genes overall on day 12 (Table II), and processes related to

replication and ribosome biogenesis were among those, which were downregulated upon drought but did not return to well-watered levels after rewatering (Fig. 5, cluster 7). Apparently, after 2 d, the expression levels of genes involved in primary production are increased however transcript levels of growth-related genes (e.g. genes involved in replication, translation, and cell division) have not yet completely recovered. This might be due to the fact that the full resource availability has not been restored within two days reflected by the still altered starch and metabolite pools (Fig. 2).

Regulation of the Coordinated Drought Response

Clustering differential gene expression indicated that the response of *T. triangulare* is multilayered since clusters respond and recover at different time points to different degrees (Fig. 3). Initially, drought stress induced a general stress response (clusters 4 and 9, Fig. 5) and a specific ABA-mediated response (cluster 5, Fig. 5; Supplemental Fig. S8). A conceptual model integrating the transcriptomic data is depicted in Figure 6. The general stress response included the CBFs, which are known to bind the drought responsive element (Zhu, 2002). However, their upregulation was transient and no longer detectable on day 12 of water limitation (Supplemental Dataset S6). During this initial stress response, our data indicate changes of the endomembrane system (cluster 9, Fig. 5). In contrast, the ABA-mediated response was further increased on day 12 (cluster 5, Fig. 5). The transcriptomic response also indicated a feed-forward loop with higher expression of

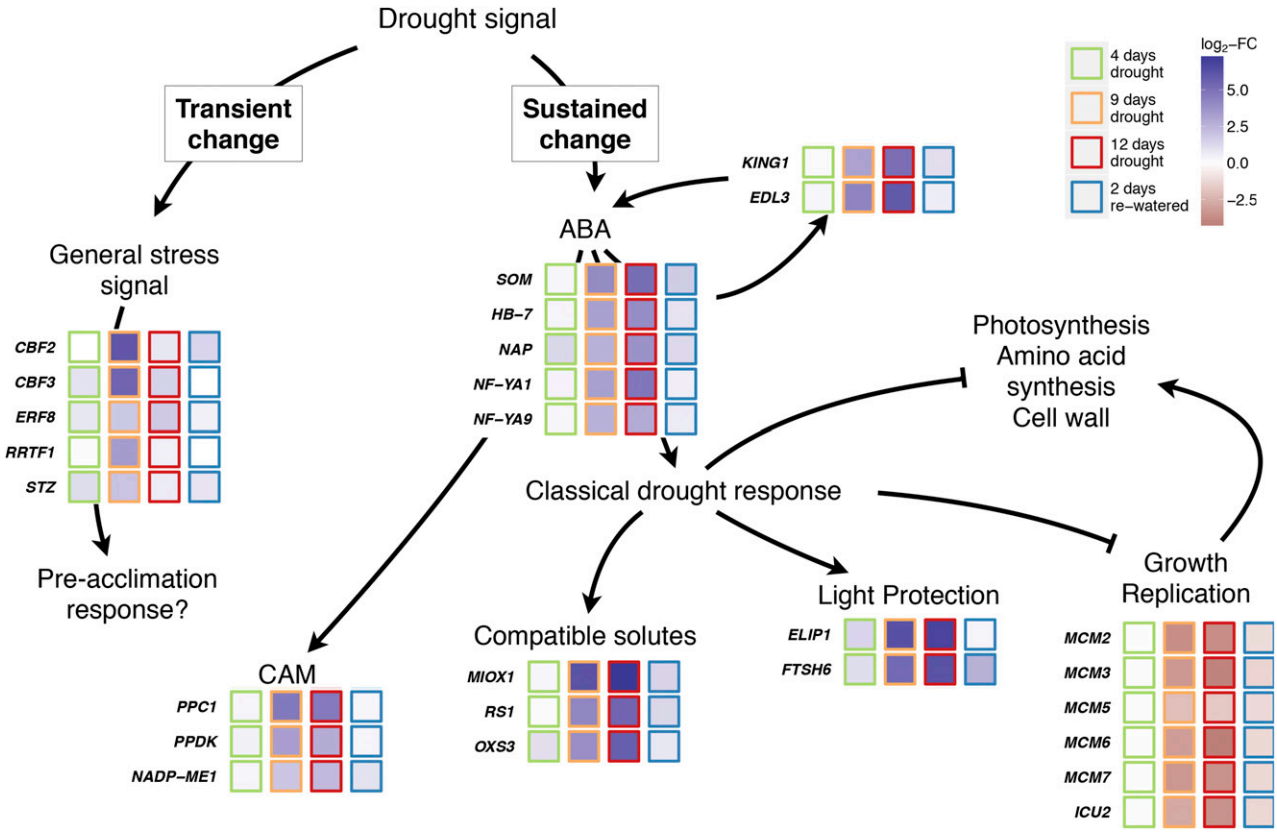

Figure 6. Proposed regulation of the coordinated drought response in *T. triangulare*. Shown are genes discussed in the text. A general stress signal was mediated by transcription factors, which were transiently upregulated on day 9 (*CBF2, C-repeat/DRE binding factor 2*; *CBF3, C-repeat/DRE binding factor 3*; *ERF8, ethylene response factor 8*; *RRTF1, redox responsive transcription factor 1*; *STZ, salt tolerance zinc finger*) and triggered a yet unclear response. The sustained response to persistent drought was primarily mediated via ABA, the activity of which was maintained through a feed-forward loop (*KING1, SNF1-related protein kinase regulatory subunit gamma 1*; *EDL3, EID1-like 3*), through ABA-responsive transcription factors (*SOM, SOMNUS*; *HB-7, homeobox 7*; *NAP, NAC-like, activated by AP3/PI*; *NF-YA1, nuclear factor Y subunit A1*; *NF-YA9, nuclear factor Y subunit A9*) and besides the induction of CAM (see Fig. 3 for details; *PPC1, phosphoenolpyruvate carboxylase 1*; *PPDK, Pyruvate phosphate dikinase, PEP/pyruvate binding domain*; *NADP-ME1, NADP-malic enzyme 1*) included a classical drought response, i.e. synthesis of compatible solutes (*RS1, Raffinose synthase 1*; *MIOX1, myoinositol oxygenase 1*; *OXS3, oxidative stress 3*) and light protection (*ELIP1, Early light inducible protein 1*; *FTSH6, FTSH protease 6*). At the same time, growth was repressed through downregulation of the replication cassette (*MCMs, minichromosome maintenance*; *ICU2, incurvata 2*) and processes related to photosynthesis, amino acid synthesis, and cell wall synthesis (see Fig. 5 and Supplemental Fig. S4) allowing *T. triangulare* to engage in a state of quiescence during drought. Log_2-FC, Absolute maximum log_2-fold changes in gene expression compared to day 0 at midday or midnight.

KING1, which activates ABA signaling, and EDL3, which mediates ABA signaling (Table I). At the same time, the expression of a PP2C was increased (expression rank 424 on day 12 at midnight, Supplemental Dataset S1), which is required to attenuate the signaling pathway once the stress signal is removed (Umezawa et al., 2009). Hence, *T. triangulare* plants are transcriptionally enabled to both sustain the ABA signal to the transcriptome and also to switch it off once the stress is removed upon rewatering. The ABA signal is likely overlaid with a carbon starvation signal. This additional signal may explain why several clusters did not recover to well-watered expression levels although soil moisture was restored. Catabolism-related processes only recovered partially (Fig. 5, clusters 3 and 5), and replication and ribosome biogenesis related genes recovered only marginally (Fig. 5, cluster 7).

The candidate transcription factors downstream of the initial signal, which is probably at least in part ABA mediated, are those that are significantly upregulated with a large magnitude. They include highly induced ABA-dependent transcription factors, such as HB7, NF-YA1 and 9, or NAP (Table IV), as well as the phosphorylation-controlled ABA-dependent transcription factors not detectable in the transcriptome analysis. Stalled growth, which is part of the response, may also at least in part be dependent on ABA as SOM is highly induced upon drought (Table I; Lim et al., 2013). SOM is required to control germination cessation in seeds downstream of the signal perception cascade (Kim et al., 2008) and thus likely controls effector genes required for growth. The trehalose-phosphate and SnRK1 mediated signaling (Baena-Gonzalez et al., 2007) does not significantly overlap with the signals observed in *T. triangulare.*

CONCLUSION

This study showed that the response of *T. triangulare* to drought stress was associated with profound and reversible changes in the transcriptome. Known key enzymes of the CAM-cycle and some of those connected to carbohydrate metabolism were upregulated, as were genes encoding functions associated with a classical drought response, including light protection and the synthesis of compatible solutes. Genes related to growth, photosynthesis, the synthesis of cell walls, and amino acids were downregulated in response to drought while catabolic processes were upregulated. A set of transcription factors likely to be involved in mediating these responses was identified. *T. triangulare* is easy to grow, flowers and produces seeds within few weeks after germination, and rapidly induces CAM in response to drought stress, thereby exhibiting important attributes of a potential model system to study key components of a drought response that includes CAM and its signaling components under stress. Research on *T. triangulare* may in the future contribute to engineering drought coping strategies such as CAM via synthetic biology into C_3 crop plants with the goal to improve their performance in water-limited environments (Yang et al., 2015).

MATERIALS AND METHODS

Plant Material and Growth Conditions

Talinum triangulare plants were grown in Miracle-Gro Potting Mix (Miracle-Gro) in "Short-One" treepots, 1.6 l (Stuewe and Sons). The experiment was initiated with 28-d-old plants in a controlled environment chamber (Environmental Growth Chambers) maintained under 12 h light (30°C, 37% relative humidity)/12 h dark (22°C) cycles. Photon flux density at leaf level was 425 μmol m^{-2} s^{-1}. Irrigation was withheld on day 1 and recommenced on day 14. Leaves were harvested when plants were well-watered as well as after 4, 9, and 12 d of water deprivation and watered for two days following the drought period.

Titratable Acidity

Mature leaves of the same plants used for RNASeq and metabolite profiling were harvested at the end of the light and dark periods, respectively, and frozen in liquid nitrogen after measurement of fresh weight. Organic acids were extracted by sequentially boiling leaves in 50% methanol and water. Titratable acidity was determined by measuring the volume of 5 mM KOH required to neutralize the aqueous extract to pH 6.5.

Metabolite Profiling

Lyophilized leaf material was extracted for metabolite analysis by gas chromatography-mass spectrometry (GC-MS) according to Fiehn et al. (2000) using a 7200 GC-QTOF (Agilent). Data analysis was conducted with the Mass Hunter Software (Agilent). For relative quantification, all metabolite peak areas were normalized to the peak area of the internal standard ribitol added prior to extraction.

RNA Extraction, Preparation, and Sequencing of Illumina Libraries

The topmost mature unshaded leaves (of approximately 3–4.5 cm length) of *T. triangulare* were harvested in the middle of the light or the middle of the dark period and immediately frozen in liquid nitrogen. RNA was isolated from ground tissue using the GeneMatrix Universal RNA Purification Kit (EURx Ltd.). Residues of DNA were removed with DNase (New England Biolabs). RNA integrity, sequencing library, and fragment size were analyzed on a 2100 Bioanalyzer (Agilent). Libraries were prepared using the TruSeq RNA Sample Prep Kit v2 (Illumina) and quantified with a Qubit 2.0 (Invitrogen). Samples were multiplexed with 12 libraries per lane and sequenced in single-end mode (Rapid Run, 150 bp read length) on an Illumina HiSEquation 2000 platform, yielding ~14 million reads per library.

Contig Assembly and Sequence Alignment

To substantiate cross-species mapping against the sequenced reference genome of Arabidopsis, Illumina libraries from representative samples (day 0, day 9, and 2 d after rewatering) were pooled and paired-end sequenced (Rapid Run, 100 bp read length) on an Illumina HiSEquation 2000 platform for assembly of contigs. Trinity assembly of the reads using Trinity (Grabherr et al., 2011) in default mode yielded 105,520 contigs, which were collapsed to 39,781 putative open reading frames using Transdecoder (transdecoder.github.io) and manual removal of duplicated contigs. Remapping placed 81% of the original 150bp reads on the ORFs. Contigs were annotated via BlastX implemented in BLAST+ (Camacho et al., 2009) against peptide sequences of the *Beta vulgaris* reference genome RefBeet-1.1 (Dohm et al., 2014) and peptide sequences of a minimal set of the TAIR10 release of the Arabidopsis genome (http://www.arabidopsis.org/). Protein sequences were aligned using Clustal Omega at www.ebi.ac.uk (Sievers et al., 2011). Phylogenetic analyses were performed with the PhyML tool (Guindon et al., 2010) implemented in SeaView 4 (Gouy et al., 2010) in default mode after Gblocks creation with the least stringent parameters.

Read Mapping and Gene Expression Profiling

Illumina reads were aligned to a minimal set of coding sequences of the TAIR 10 release of the Arabidopsis genome (http://www.arabidopsis.org/) using BLAT (Kent, 2002) in protein space. The minimal transcriptome was obtained as described in Gowik et al. (2011) and contains 21,869 nuclear encoded protein-coding genes. The best BLAT hit for each read was determined by (1) lowest e-value and (2) highest bit score. Raw read counts were transformed to reads per million (rpm) to normalize for the number of reads available at each sampling stage. Cross-species mapping takes advantage of the completeness and annotation of the Arabidopsis genome and overcomes the limitations of transcriptome assembly (Franssen et al., 2011; Schliesky et al., 2012). To quantify abundance of contigs, the 150 bp single-end reads were mapped onto the assembled contigs using the RNA-Seq analysis tool implemented in the CLC genomics workbench version 8.5 (www.clcbio.com) in default mode.

Data Analysis

Data analysis was performed using R statistics software (R version 3.2.1 provided by the CRAN project, http://www.R-project.org). Differential gene expression was analyzed with the DESeq2 package (Love et al., 2014) in default mode. Automatic independent filtering retained 16,766 genes with nonzero total read count. A significance threshold of 0.01 was applied after p-value adjustment with false discovery rate via Benjamini-Hochberg correction (Benjamini and Hochberg, 1995). Log_2 expression ratios calculated by DESeq2 were used for downstream analysis. For *k*-means clustering, transcript levels were log_2-transformed and scaled via calculation of z-scores by gene. One *k*-means clustering was performed for each daytime of sampling (MD and MN) by R statistics software with 6,800 (MD) and 7,563 (MN) genes that were determined as differentially expressed genes (DEG) compared to well-watered (day 0), respectively. Enrichment for GO terms of biological processes within *k*-means clusters was performed via Fisher's Exact Test implemented in the R-package topGO (Alexa et al., 2006; including DEG as the background set, significance level of alpha = 0.01). All log_2-fold changes of water-limited days compared to day 0 were used for pathway analysis in Mapman (Thimm et al., 2004). Wilcoxon Rank Sum test implemented in Mapman was used to test for enrichment and corrected for multiple hypothesis testing via Benjamini-Hochberg correction (Benjamini and Hochberg, 1995). Arabidopsis response to treatments with the phytohormones ABA, 1-aminocyclopropane-1-carboxylic acid (a precursor of ethylene), brassinolide (a brassinosteroid), indole-3-acetic acid (i.e. auxin), and zeatin (a cytokinine) were extracted from AtGenExpress and are based on microarrays by Goda et al. (2008). Response to hormone treatment ($n = 3$) compared to mock treatment ($n = 3$) was called significant at $q < 0.01$ (corrected after Benjamini and Hochberg [1995]). Overlap of *T. triangulare* reponse to drought with Arabidopsis response to hormone treatments was calculated using Fisher's Exact Test ($p < 0.001$). All log_2-fold changes (treatment vs. mock) of Arabidopsis response to ABA treatment (Goda et al., 2008) were used for pathway analysis in Mapman. Data were annotated with publicly available information for Arabidopsis (TAIR10, http://www.arabidopsis.org/). Full quantitative data with annotation is available as Supplemental Dataset S1.

Accession Number

The read data have been submitted to the National Center for Biotechnology Information Gene Expression Omnibus under accession number GSE70601 (http://www.ncbi.nlm.nih.gov/geo/query/acc.cgi?token=wryvugcifxexnml&acc=GSE70601).

Supplemental Data

The following supplemental materials are available.

Supplemental Data Set S1. Quantitative information and annotation for all reads mapped onto the reference genome of Arabidopsis.

Supplemental Data Set S2. Quantitative information and annotation for all reads mapped onto the *Talinum* contigs.

Supplemental Data Set S3. Levels of all putative CAM genes sensu stricto and sensu lato.

Supplemental Data Set S4. Enriched Mapman categories for all plants harvested 4, 9, and 12 d after water deprivation and 2 d after rewatering (re2) at the middle of the day (MD) or night (MN).

Supplemental Data Set S5. Full list of enriched GO terms in *k*-means clusters (Fig. 5; Supplemental Fig. S7).

Supplemental Data Set S6. Transcription factors differentially expressed on day 9 and/or day 12.

Supplemental Figure S1. Changes in leaf transcriptomes and metabolomes under varying levels of water availability in the middle of the night (analogous to Fig. 1, B and C).

Supplemental Figure S2. *T. triangulare* PEPCs show characteristics of both C_3 and C_4 plants.

Supplemental Figure S3. *Talinum* NADP-ME with highest transcript are predicted to be localized in the plastid.

Supplemental Figure S4. Levels of photorespiratory metabolites.

Supplemental Figure S5. Levels of compatible solutes.

Supplemental Figure S6. Mapman overview of metabolism for all drought samples (day 4, day 9, and day 12 of water deprivation and 2 d after rewatering [re2] compared to day 0).

Supplemental Figure S7. *K*-means clustering of relative gene expression at the middle of the night.

Supplemental Figure S8. Overlap of differentially expressed genes during CAM in *T. triangulare* with hormone treated leaves of Arabidopsis (Goda et al., 2008).

Supplemental Figure S9. Mapman overview of metabolism for ABA response in Arabidopsis.

Supplemental Figure S10. Experiments to assay activity of NADP-ME (panels 1–4) or MDH (panel 5) with leaf extracts of *T. triangulare* ("*Talinum* extract") or recombinant NADP-ME from *Z. mays* (ZmNADP-ME, provided by Anastasiia Bovdilova, group of Veronica G. Maurino).

Supplemental Figure S11. Levels of additional metabolites.

Supplemental Table S1. mRNA-Seq statistics.

Supplemental Table S2. Metabolite profiling statistics.

Supplemental Table S3. Expression levels of *T. triangulare* contigs encoding PEPC.

Supplemental Table S4. Expression levels of all *T. triangulare* contigs encoding for subunits of vacuolar ATP synthases.

Supplemental Table S5. Expression levels of *T. triangulare* contigs encoding NADP-ME.

Supplemental Table S6. Expression levels of two *T. triangulare* contigs encoding PPDK.

Supplemental Table S7. Expression levels of genes encoding for photorespiratory enzymes.

Supplemental Table S8. Estimated partitioning of carbon in organic acids and starch on day 12.

ACKNOWLEDGMENTS

We acknowledge the excellent technical assistance of M. Graf, K. Weber, and E. Klemp for GC-MS measurements, S. Kurz for help with Illumina library preparation, and A. Virgo for titration of organic acids.

Received July 22, 2015; accepted November 3, 2015; published November 3, 2015.

LITERATURE CITED

Alexa A, Rahnenführer J, Lengauer T (2006) Improved scoring of functional groups from gene expression data by decorrelating GO graph structure. Bioinformatics **22:** 1600–1607

Ashton AR, Burnell JN, Furbank RT, Jenkins CLD, Hatch MD (1990) 3 enzymes of C4 photosynthesis. Enzymes of Primary Metabolism **3:** 39

Baena-González E, Rolland F, Thevelein JM, Sheen J (2007) A central integrator of transcription networks in plant stress and energy signalling. Nature **448:** 938–942

Bartels D, Sunkar R (2005) Drought and salt tolerance in plants. Crit Rev Plant Sci **24:** 23–58

Benjamini Y, Hochberg Y (1995) Controlling the false discovery rate - a practical and powerful approach to multiple testing. J R Stat Soc, B **57:** 289–300

Bläsing OE, Westhoff P, Svensson P (2000) Evolution of C4 phospho*enol*pyruvate carboxylase in *Flaveria*, a conserved serine residue in the carboxyl-terminal part of the enzyme is a major determinant for C4-specific characteristics. J Biol Chem **275:** 27917–27923

Bohnert HJ, Nelson DE, Jensen RG (1995) Adaptations to environmental stresses. Plant Cell **7:** 1099–1111

Borland AM, Barrera Zambrano VA, Ceusters J, Shorrock K (2011) The photosynthetic plasticity of crassulacean acid metabolism: an evolutionary innovation for sustainable productivity in a changing world. New Phytol **191:** 619–633

Borland AM, Hartwell J, Jenkins GI, Wilkins MB, Nimmo HG (1999) Metabolite control overrides circadian regulation of phospho*enol*pyruvate carboxylase kinase and CO2 fixation in crassulacean acid metabolism. Plant Physiol **121:** 889–896

Bray EA (1997) Plant responses to water deficit. Trends Plant Sci **2:** 48–54

Bräutigam A, Hoffmann-Benning S, Weber AP, Weber APM (2008) Comparative proteomics of chloroplast envelopes from C3 and C4 plants reveals specific adaptations of the plastid envelope to C4 photosynthesis and candidate proteins required for maintaining C4 metabolite fluxes. Plant Physiol **148:** 568–579

Bräutigam A, Kajala K, Wullenweber J, Sommer M, Gagneul D, Weber KL, Carr KM, Gowik U, Mass J, Lercher MJ, et al (2011) An mRNA blueprint for C4 photosynthesis derived from comparative transcriptomics of closely related C3 and C4 species. Plant Physiol **155:** 142–156

Bräutigam A, Schliesky S, Külahoglu C, Osborne CP, Weber APM (2014) Towards an integrative model of C4 photosynthetic subtypes: insights from comparative transcriptome analysis of NAD-ME, NADP-ME, and PEP-CK C4 species. J Exp Bot **65:** 3579–3593

Camacho C, Coulouris G, Avagyan V, Ma N, Papadopoulos J, Bealer K, Madden TL (2009) BLAST+: architecture and applications. BMC Bioinformatics **10:** 421

Carter PJ, Nimmo HG, Fewson CA, Wilkins MB (1991) Circadian rhythms in the activity of a plant protein kinase. EMBO J **10:** 2063–2068

Chaves MM, Maroco J, Pereira JS (2003) Understanding plant responses to drought - from genes to the whole plant. Funct Plant Biol **30:** 239–264

Cheffings CM, Pantoja O, Ashcroft FM, Smith JA (1997) Malate transport and vacuolar ion channels in CAM plants. J Exp Bot **48:** 623–631

Chia T, Thorneycroft D, Chapple A, Messerli G, Chen J, Zeeman SC, Smith SM, Smith AM (2004) A cytosolic glucosyltransferase is required for conversion of starch to sucrose in Arabidopsis leaves at night. Plant J **37:** 853–863

Christin P-A, Arakaki M, Osborne CP, Bräutigam A, Sage RF, Hibberd JM, Kelly S, Covshoff S, Wong GK-S, Hancock L, et al (2014) Shared origins of a key enzyme during the evolution of C4 and CAM metabolism. J Exp Bot **65:** 3609–3621

Cushman JC, Agarie S, Albion RL, Elliot SM, Taybi T, Borland AM (2008a) Isolation and characterization of mutants of common ice plant deficient in crassulacean acid metabolism. Plant Physiol **147:** 228–238

Cushman JC, Tillett RL, Wood JA, Branco JM, Schlauch KA (2008b) Large-scale mRNA expression profiling in the common ice plant, *Mesembryanthemum crystallinum*, performing C3 photosynthesis and Crassulacean acid metabolism (CAM). J Exp Bot **59:** 1875–1894

Cutler SR, Rodriguez PL, Finkelstein RR, Abrams SR (2010) Abscisic acid: emergence of a core signaling network. Annu Rev Plant Biol **61:** 651–679

Dever LV, Boxall SF, Kneřová J, Hartwell J (2015) Transgenic perturbation of the decarboxylation phase of Crassulacean acid metabolism alters physiology and metabolism but has only a small effect on growth. Plant Physiol **167:** 44–59

Dittrich P (1976) Nicotinamide adenine dinucleotide-specific "malic" enzyme in *Kalanchoë daigremontiana* and other plants exhibiting crassulacean acid metabolism. Plant Physiol **57:** 310–314

Dohm JC, Minoche AE, Holtgräwe D, Capella-Gutiérrez S, Zakrzewski F, Tafer H, Rupp O, Sörensen TR, Stracke R, Reinhardt R, et al (2014) The genome of the recently domesticated crop plant sugar beet (*Beta vulgaris*). Nature **505:** 546–549

Elbein AD, Pan YT, Pastuszak I, Carroll D (2003) New insights on trehalose: a multifunctional molecule. Glycobiology **13:** 17R–27R

Emanuelsson O, Nielsen H, Brunak S, von Heijne G (2000) Predicting subcellular localization of proteins based on their N-terminal amino acid sequence. J Mol Biol **300:** 1005–1016

Fiehn O, Kopka J, Dörmann P, Altmann T, Trethewey RN, Willmitzer L (2000) Metabolite profiling for plant functional genomics. Nat Biotechnol **18:** 1157–1161

Findling S, Zanger K, Krueger S, Lohaus G (2015) Subcellular distribution of raffinose oligosaccharides and other metabolites in summer and winter leaves of *Ajuga reptans* (*Lamiaceae*). Planta **241:** 229–241

Flexas J, Bota J, Galmés J, Medrano H, Ribas-Carbó M (2006) Keeping a positive carbon balance under adverse conditions: responses of photosynthesis and respiration to water stress. Physiol Plant **127:** 343–352

Franssen SU, Shrestha RP, Bräutigam A, Bornberg-Bauer E, Weber APM (2011) Comprehensive transcriptome analysis of the highly complex *Pisum sativum* genome using next generation sequencing. BMC Genomics **12:** 227–242

Furumoto T, Yamaguchi T, Ohshima-Ichie Y, Nakamura M, Tsuchida-Iwata Y, Shimamura M, Ohnishi J, Hata S, Gowik U, Westhoff P, et al (2011) A plastidial sodium-dependent pyruvate transporter. Nature **476:** 472–475

Goda H, Sasaki E, Akiyama K, Maruyama-Nakashita A, Nakabayashi K, Li W, Ogawa M, Yamauchi Y, Preston J, Aoki K, et al (2008) The AtGenExpress hormone and chemical treatment data set: experimental design, data evaluation, model data analysis and data access. Plant J **55:** 526–542

Gouy M, Guindon S, Gascuel O (2010) SeaView version 4: A multiplatform graphical user interface for sequence alignment and phylogenetic tree building. Mol Biol Evol **27:** 221–224

Gowik U, Bräutigam A, Weber KL, Weber APM, Westhoff P (2011) Evolution of C4 photosynthesis in the genus *Flaveria*: how many and which genes does it take to make C4? Plant Cell **23:** 2087–2105

Gowik U, Engelmann S, Bläsing OE, Raghavendra AS, Westhoff P (2006) Evolution of C(4) phospho*enol*pyruvate carboxylase in the genus *Alternanthera*: gene families and the enzymatic characteristics of the C(4) isozyme and its orthologues in C(3) and C(3)/C(4) *Alternantheras*. Planta **223:** 359–368

Grabherr MG, Haas BJ, Yassour M, Levin JZ, Thompson DA, Amit I, Adiconis X, Fan L, Raychowdhury R, Zeng Q, et al (2011) Full-length transcriptome assembly from RNA-Seq data without a reference genome. Nat Biotechnol **29:** 644–652

Guindon S, Dufayard J-F, Lefort V, Anisimova M, Hordijk W, Gascuel O (2010) New algorithms and methods to estimate maximum-likelihood phylogenies: assessing the performance of PhyML 3.0. Syst Biol **59:** 307–321

Haider MS, Barnes JD, Cushman JC, Borland AM (2012) A CAM- and starch-deficient mutant of the facultative CAM species *Mesembryanthemum crystallinum* reconciles sink demands by repartitioning carbon during acclimation to salinity. J Exp Bot **63:** 1985–1996

Hare PD, Cress WA, Van Staden J (1998) Dissecting the roles of osmolyte accumulation during stress. Plant Cell Environ **21:** 535–553

Harris D, Martin C (1991) Plasticity in the degree of CAM-cycling and its relationship to drought stress in 5 species of *Talinum* (*Portulacaceae*). Oecologia **86:** 575–584

Hartwell J, Gill A, Nimmo GA, Wilkins MB, Jenkins GI, Nimmo HG (1999) Phospho*enol*pyruvate carboxylase kinase is a novel protein kinase regulated at the level of expression. Plant J **20:** 333–342

Hartwell J, Smith LH, Wilkins MB, Jenkins GI, Nimmo HG (1996) Higher plant phospho*enol*pyruvate carboxylase kinase is regulated at the level of translatable mRNA in response to light or a circadian rhythm. Plant J **10:** 1071–1078

Häusler RE, Baur B, Scharte J, Teichmann T, Eicks M, Fischer KL, Flügge U-I, Schubert S, Weber A, Fischer K (2000) Plastidic metabolite transporters and their physiological functions in the inducible crassulacean acid metabolism plant *Mesembryanthemum crystallinum*. Plant J **24:** 285–296

Heddad M, Adamska I (2000) Light stress-regulated two-helix proteins in *Arabidopsis thaliana* related to the chlorophyll a/b-binding gene family. Proc Natl Acad Sci USA **97:** 3741–3746

Herrera A (1999) Effects of photoperiod and drought on the induction of *Crassulacean* acid metabolism and the reproduction of plants of *Talinum triangulare*. Can J Bot **77:** 404–409

Herrera A (2009) Crassulacean acid metabolism and fitness under water deficit stress: if not for carbon gain, what is facultative CAM good for? Ann Bot (Lond) **103:** 645–653

Herrera A, Ballestrini C, Montes E (2015) What is the potential for dark CO2 fixation in the facultative crassulacean acid metabolism species *Talinum triangulare?* J Plant Physiol **174:** 55–61

Herrera A, Delgado J, Paraguatey I (1991) Occurrence of inducible crassulacean acid metabolism in leaves of *Talinum triangulare* (*Portulacaceae*). J Exp Bot **42:** 493–499

Holtum JAM, Smith JAC, Neuhaus HE (2005) Intracellular transport and pathways of carbon flow in plants with crassulacean acid metabolism. Funct Plant Biol **32:** 429–449

Holtum JAM, Winter K (1982) Activity of enzymes of carbon metabolism during the induction of Crassulacean acid metabolism in *Mesembryanthemum crystallinum* L. Planta **155:** 8–16

Hutin C, Nussaume L, Moise N, Moya I, Kloppstech K, Havaux M (2003) Early light-induced proteins protect *Arabidopsis* from photooxidative stress. Proc Natl Acad Sci USA **100:** 4921–4926

Ingram J, Bartels D (1996) The molecular basis of dehydration tolerance in plants. Annu Rev Plant Physiol Plant Mol Biol **47:** 377–403

Kent WJ (2002) BLAT - The BLAST-like alignment tool. Genome Res **12:** 656–664

Kim DH, Yamaguchi S, Lim S, Oh E, Park J, Hanada A, Kamiya Y, Choi G (2008) SOMNUS, a CCCH-type zinc finger protein in *Arabidopsis*, negatively regulates light-dependent seed germination downstream of PIL5. Plant Cell **20:** 1260–1277

Kluge M, Osmond CB (1971) Pyruvate Pi dikinase in crassulacean acid metabolism. Naturwissenschaften **58:** 414–415

Kollist H, Nuhkat M, Roelfsema MRG (2014) Closing gaps: linking elements that control stomatal movement. New Phytol **203:** 44–62

Kondo A, Nose A, Ueno O (2001) Coordinated accumulation of the chloroplastic and cytosolic pyruvate, Pi dikinases with enhanced expression of CAM in *Kalanchoë blossfeldiana*. Physiol Plant **111:** 116–122

Kore-eda S, Noake C, Ohishi M, Ohnishi J, Cushman JC (2005) Transcriptional profiles of organellar metabolite transporters during induction of Crassulacean acid metabolism in *Mesembryanthemum crystallinum*. Funct Plant Biol **32:** 451–466

Lawlor DW, Cornic G (2002) Photosynthetic carbon assimilation and associated metabolism in relation to water deficits in higher plants. Plant Cell Environ **25:** 275–294

Lim S, Park J, Lee N, Jeong J, Toh S, Watanabe A, Kim J, Kang H, Kim DH, Kawakami N, et al (2013) ABA-insensitive3, ABA-insensitive5, and DELLAs interact to activate the expression of SOMNUS and other high-temperature-inducible genes in imbibed seeds in Arabidopsis. Plant Cell **25:** 4863–4878

Liu Q, Kasuga M, Sakuma Y, Abe H, Miura S, Yamaguchi-Shinozaki K, Shinozaki K (1998) Two transcription factors, DREB1 and DREB2, with an EREBP/AP2 DNA binding domain separate two cellular signal transduction pathways in drought- and low-temperature-responsive gene expression, respectively, in Arabidopsis. Plant Cell **10:** 1391–1406

Lobell DB, Gourdji SM (2012) The influence of climate change on global crop productivity. Plant Physiol **160:** 1686–1697

Love MI, Huber W, Anders S (2014) Moderated estimation of fold change and dispersion for RNA-seq data with DESeq2. Genome Biol **15:** 550–570

Lüttge U (2002) CO_2-concentrating: consequences in crassulacean acid metabolism. J Exp Bot **53:** 2131–2142

Lüttge U (2011) Photorespiration in phase III of crassulacean acid metabolism: evolutionary and ecophysiological implications. Prog Bot **72:** 371–384

Nägele T, Heyer AG (2013) Approximating subcellular organisation of carbohydrate metabolism during cold acclimation in different natural accessions of *Arabidopsis thaliana*. New Phytol **198:** 777–787

Niewiadomska E, Borland AM (2007) Crassulacean acid metabolism: a cause or consequence of oxidative stress in planta? Prog Bot **69:** 247–266

Niittylä T, Messerli G, Trevisan M, Chen J, Smith AM, Zeeman SC (2004) A previously unknown maltose transporter essential for starch degradation in leaves. Science **303:** 87–89

Nishizawa A, Yabuta Y, Shigeoka S (2008) Galactinol and raffinose constitute a novel function to protect plants from oxidative damage. Plant Physiol **147:** 1251–1263

Noctor G, Foyer CH (2000) Homeostasis of adenylate status during photosynthesis in a fluctuating environment. J Exp Bot **51:** 347–356

Osmond CB (1978) Crassulacean acid metabolism: a curiosity in context. Annu Rev Plant Physiol **29:** 379–414

Park S-Y, Fung P, Nishimura N, Jensen DR, Fujii H, Zhao Y, Lumba S, Santiago J, Rodrigues A, Chow T-FF, et al (2009) Abscisic acid inhibits type 2C protein phosphatases via the PYR/PYL family of START proteins. Science **324:** 1068–1071

Parsley K, Hibberd JM (2006) The *Arabidopsis* PPDK gene is transcribed from two promoters to produce differentially expressed transcripts responsible for cytosolic and plastidic proteins. Plant Mol Biol **62:** 339–349

Paulus JK, Schlieper D, Groth G (2013) Greater efficiency of photosynthetic carbon fixation due to single amino-acid substitution. Nat Commun **4:** 1518–1524

Pérez-Rodríguez P, Riaño-Pachón DM, Corrêa LGG, Rensing SA, Kersten B, Mueller-Roeber B (2010) PlnTFDB: updated content and new features of the plant transcription factor database. Nucleic Acids Res **38:** D822–D827

Sage RF (2003) The evolution of C4 photosynthesis. New Phytol **161:** 341–370

Sakamoto H, Araki T, Meshi T, Iwabuchi M (2000) Expression of a subset of the Arabidopsis Cys(2)/His(2)-type zinc-finger protein gene family under water stress. Gene **248:** 23–32

Sakamoto H, Maruyama K, Sakuma Y, Meshi T, Iwabuchi M, Shinozaki K, Yamaguchi-Shinozaki K (2004) Arabidopsis Cys2/His2-type zinc-finger proteins function as transcription repressors under drought, cold, and high-salinity stress conditions. Plant Physiol **136:** 2734–2746

Schliesky S, Gowik U, Weber APM, Bräutigam A (2012) RNA-Seq assembly - Are we there yet? Front Plant Sci **3:** 220

Sievers F, Wilm A, Dineen D, Gibson TJ, Karplus K, Li W, Lopez R, McWilliam H, Remmert M, Söding J, et al (2011) Fast, scalable generation of high-quality protein multiple sequence alignments using Clustal Omega. Mol Syst Biol **7:** 539–544

Smith SM, Fulton DC, Chia T, Thorneycroft D, Chapple A, Dunstan H, Hylton C, Zeeman SC, Smith AM (2004) Diurnal changes in the transcriptome encoding enzymes of starch metabolism provide evidence for both transcriptional and posttranscriptional regulation of starch metabolism in *Arabidopsis* leaves. Plant Physiol **136:** 2687–2699

Streb S, Zeeman SC (2012) Starch metabolism in Arabidopsis. The Arabidopsis Book **10:** doi/10.199/tab.e0160

Sun J, Jiang H, Xu Y, Li H, Wu X, Xie Q, Li C (2007) The CCCH-type zinc finger proteins AtSZF1 and AtSZF2 regulate salt stress responses in *Arabidopsis*. Plant Cell Physiol **48:** 1148–1158

Svensson P, Bläsing OE, Westhoff P (1997) Evolution of the enzymatic characteristics of C4 phospho*enol*pyruvate carboxylase–a comparison of the orthologous PPCA phospho*enol*pyruvate carboxylases of *Flaveria trinervia* (C4) and *Flaveria pringlei* (C3). Eur J Biochem **246:** 452–460

Svensson P, Bläsing OE, Westhoff P (2003) Evolution of C4 phospho*enol*pyruvate carboxylase. Arch Biochem Biophys **414:** 180–188

Taisma MA, Herrera A (1998) A relationship between fecundity, survival, and the operation of crassulacean acid metabolism in *Talinum triangulare*. Can J Bot **76:** 1908–1915

Taisma MA, Herrera A (2003) Drought under natural conditions affects leaf properties, induces CAM and promotes reproduction in plants of *Talinum triangulare*. Interciencia **28:** 292–297

Taybi T, Cushman JC (2002) Abscisic acid signaling and protein synthesis requirements for phospho*enol*pyruvate carboxylase transcript induction in the common ice plant. J Plant Physiol **159:** 1235–1243

Taybi T, Nimmo HG, Borland AM (2004) Expression of phospho*enol*pyruvate carboxylase and phospho*enol*pyruvate carboxylase kinase genes. Implications for genotypic capacity and phenotypic plasticity in the expression of crassulacean acid metabolism. Plant Physiol **135:** 587–598

Taybi T, Patil S, Chollet R, Cushman JC (2000) A minimal serine/threonine protein kinase circadianly regulates phospho*enol*pyruvate carboxylase activity in crassulacean acid metabolism-induced leaves of the common ice plant. Plant Physiol **123:** 1471–1482

Taybi T, Sotta B, Gehrig H, Guclu S, Kluge M, Brulfert J (1995) Differential effects of abscisic acid on phospho*enol*pyruvate carboxylase and CAM operation in *Kalanchoë blossfeldiana*. Bot Acta **108:** 240–246

Thimm O, Bläsing O, Gibon Y, Nagel A, Meyer S, Krüger P, Selbig J, Müller LA, Rhee SY, Stitt M (2004) MAPMAN: a user-driven tool to display genomics data sets onto diagrams of metabolic pathways and other biological processes. Plant J **37:** 914–939

Tsuzuki M, Miyachi S, Winter K, Edwards GE (1982) Localization of carbonic anhydrase in crassulacean acid metabolism plants. Plant Sci Lett **24:** 211–218

Umezawa T, Sugiyama N, Mizoguchi M, Hayashi S, Myouga F, Yamaguchi-Shinozaki K, Ishihama Y, Hirayama T, Shinozaki K (2009) Type 2C protein phosphatases directly regulate abscisic acid-activated protein kinases in *Arabidopsis*. Proc Natl Acad Sci USA **106:** 17588–17593

Weber A, Servaites JC, Geiger DR, Kofler H, Hille D, Gröner F, Hebbeker U, Flügge U-I (2000) Identification, purification, and molecular cloning of a putative plastidic glucose translocator. Plant Cell **12:** 787–802

Weise SE, van Wijk KJ, Sharkey TD (2011) The role of transitory starch in C(3), CAM, and C(4) metabolism and opportunities for engineering leaf starch accumulation. J Exp Bot **62:** 3109–3118

White PJ, Smith JA (1989) Proton and anion transport at the tonoplast in crassulacean-acid-metabolism plants: specificity of the malate-influx system in *Kalanchoë daigremontiana.* Planta **179:** 265–274

Wilson RL, Kim H, Bakshi A, Binder BM (2014) The ethylene receptors ETHYLENE RESPONSE1 and ETHYLENE RESPONSE2 have contrasting roles in seed germination of Arabidopsis during salt stress. Plant Physiol **165:** 1353–1366

Winter K, Foster JG, Edwards GE, Holtum JAM (1982) Intracellular localization of enzymes of carbon metabolism in *Mesembryanthemum crystallinum* exhibiting C_3 photosynthesic characteristics or performing Crassulacean acid metabolism. Plant Physiol **69:** 300–307

Winter K, Garcia M, Holtum JAM (2008) On the nature of facultative and constitutive CAM: environmental and developmental control of CAM expression during early growth of *Clusia, Kalanchöe*, and *Opuntia.* J Exp Bot **59:** 1829–1840

Winter K, Holtum JAM (2007) Environment or development? Lifetime net CO_2 exchange and control of the expression of Crassulacean acid metabolism in *Mesembryanthemum crystallinum.* Plant Physiol **143:** 98–107

Winter K, Holtum JAM (2014) Facultative crassulacean acid metabolism (CAM) plants: powerful tools for unravelling the functional elements of CAM photosynthesis. J Exp Bot **65:** 3425–3441

Winter K, Smith JAC (1996) An introduction to crassulacean acid metabolism. Biochemical principles and ecological diversity. *In* Crassulacean Acid Metabolism. Springer, Berlin Germany, pp 1–13

Winter K, von Willert DJ (1972) NaCl-induzierter Crassulaceansäurestoffwechsel bei *Mesembryanthemum crystallinum.* Z Pflanzenphysiol **67:** 166–170

Yang J, Worley E, Udvardi M (2014) A NAP-AAO3 regulatory module promotes chlorophyll degradation via ABA biosynthesis in Arabidopsis leaves. Plant Cell **26:** 4862–4874

Yang X, Cushman JC, Borland AM, Edwards EJ, Wullschleger SD, Tuskan GA, Owen NA, Griffiths H, Smith JAC, De Paoli HC, et al (2015) A roadmap for research on crassulacean acid metabolism (CAM) to enhance sustainable food and bioenergy production in a hotter, drier world. New Phytol **207:** 491–504

Zelisko A, García-Lorenzo M, Jackowski G, Jansson S, Funk C (2005) AtFtsH6 is involved in the degradation of the light-harvesting complex II during high-light acclimation and senescence. Proc Natl Acad Sci USA **102:** 13699–13704

Zhu J-K (2002) Salt and drought stress signal transduction in plants. Annu Rev Plant Biol **53:** 247–273

Zou C, Sun K, Mackaluso JD, Seddon AE, Jin R, Thomashow MF, Shiu S-H (2011) Cis-regulatory code of stress-responsive transcription in *Arabidopsis thaliana.* Proc Natl Acad Sci USA **108:** 14992–14997